Atmos. Chem. Phys. Discuss., 13, 26389–26450, 2013
www.atmos-chem-phys-discuss.net/13/26389/2013/
doi:10.5194/acpd-13-26389-2013

Atmospheric Chemistry and Physics Discussions

Evaluation of aerosol number concentrations in NorESM with improved nucleation parameterisation

R. Makkonen[1,*], **Ø. Seland**[2], **A. Kirkevåg**[2], **T. Iversen**[1,2], **and J. E. Kristjánsson**[1]

[1]Department of Geosciences, University of Oslo, P.O. Box 1047 Blindern, 0316 Oslo, Norway
[2]Norwegian Meteorological Institute, P.O. Box 43 Blindern, 0313 Oslo, Norway
[*]now at: Department of Physics, University of Helsinki, P.O. Box 64, 00014 University of Helsinki, Finland

Received: 25 September 2013 – Accepted: 30 September 2013 – Published: 11 October 2013

Correspondence to: R. Makkonen (risto.makkonen@helsinki.fi)

Published by Copernicus Publications on behalf of the European Geosciences Union.

Abstract

The Norwegian Earth System Model (NorESM) is evaluated against atmospheric observations of aerosol number concentrations. The model is extended to include an explicit mechanism for new particle formation, and the secondary organic aerosol (SOA) formation from biogenic precursors is revised. Several model experiments are conducted to study the sensitivity of simulated number concentrations to nucleation, SOA formation, black carbon size distribution and model meteorology. Comparison against 60 measurement sites reveals that the model with improved nucleation and SOA scheme performs well in terms of correlation coefficient $R^2 = 0.41$ calculated against monthly mean observed aerosol number concentrations with a number concentration bias of −6 %. NorESM generally overestimates the amplitude of the seasonal cycle, possibly due to too high sensitivity to biogenic precursors. Simulated vertical profiles are also evaluated against 12 flight campaigns.

1 Introduction

Atmospheric aerosol particles affect climate not only by scattering and absorbing radiation, but by acting as cloud condensation nuclei (CCN) and affecting the dynamical and radiative properties of clouds. A recent multimodel effort in the AeroCom framework (Myhre et al., 2013) found anthropogenic direct radiative forcing ranging from −0.58 to $-0.02\,\mathrm{W\,m^{-2}}$, i.e. all 16 models estimate a climate cooling effect from the direct aerosol effect (scattering and absorption of radiation). However, not all aerosols are cooling: the same study by Myhre et al. (2013) found a model median direct forcing of $+0.23\,\mathrm{W\,m^{-2}}$ for black carbon (BC) from fossil fuel and biomass burning, and even $+1.1\,\mathrm{W\,m^{-2}}$ BC forcing has been suggested (Bond et al., 2013). Due to potential high gains, the mitigation of climate warming by effective reduction in black carbon has been increasingly discussed in the recent years (e.g. Anenberg et al., 2012).

ACPD
13, 26389–26450, 2013

Although anthropogenic aerosols probably contribute to a net climate cooling via aerosol direct effect, the human influence on Earth's radiative balance is likely to be even stronger via the aerosol indirect effect. The IPCC reported that the aerosol-induced modification of the cloud albedo causes a negative forcing between −2.2 to $-0.5\,\mathrm{W\,m^{-2}}$ (Forster et al., 2007), and the indirect effects beyond cloud albedo effect can be of similar magnitude (Lohmann and Feichter, 2005). Compared to the direct radiative effect, the aerosol indirect effect is more difficult to estimate by modeling. In addition to a realistic description of cloud formation, the aerosol-cloud interactions are very sensitive to the aerosol size distribution, size-segregated composition information and aerosol mixing state.

Information on aerosol size distribution and number concentration have been included in global aerosol models for more than a decade (Von Salzen et al., 2000; Ghan et al., 2001; Adams and Seinfeld, 2002). However, aerosol microdynamics are extremely difficult to model in the global scale. First, many aerosol dynamical processes, such as coagulation, are computationally demanding and need to be simplified for modeling purposes. Second, some relevant processes, such as atmospheric nucleation, remain poorly understood and constrained. Even the discretization of the aerosol population information is demanding: most global aerosol models use either modal (Stier et al., 2005; Mann et al., 2010) or sectional (Adams and Seinfeld, 2002; Spracklen et al., 2005) approaches, but the number of modes or bins is restricted by computational constraints. The degradation of aerosol size distribution information begins already at the point of emission, when models generally use simple conversions from mass to number emission. Recently however, direct aerosol number emissions have also been applied in European scale (Fountoukis et al., 2012; Kulmala et al., 2011).

Developments of global aerosol models have both improved simulated aerosol number concentrations and revealed crucial information of the relative importance of aerosol processes in the atmosphere. In terms of mass, aerosols form either by emission of primary particles or by formation of secondary aerosol material in the at-

ACPD
13, 26389–26450, 2013

mosphere. To affect particle number concentration, secondary aerosol formation must lead to the formation of a new particle via nucleation. Globally averaged, primary emissions dominate the atmospheric aerosol mass loading due to sea salt and dust emissions. With regard to particle number, however, atmospheric nucleation can explain even a major fraction of concentrations in the boundary layer, and even 99 % above 5 km (Merikanto et al., 2009). While anthropogenic emissions contribute only a small amount to the total aerosol mass, the addition to aerosol number concentration due to anthropogenic activities can be even 35 % (Makkonen et al., 2012b).

In this paper we will evaluate the aerosol number concentrations simulated by the Norwegian Earth System Model (NorESM). The model is evaluated against 60 measurement stations, aerosol measurement campaigns, vertical observations from flight campaigns and a compilation of marine aerosol number concentrations. With the help of sensitivity simulations, we investigate the relative roles of different processes and emissions affecting the simulated number concentration. The results will help assessing the performance of the aerosol dynamics in NorESM. The comparison of the sensitivity simulations will indicate the relative roles of secondary aerosol formation and primary aerosol to aerosol number concentrations.

2 Model description

2.1 NorESM1-M

The NorESM1 is one of the Earth System Models participating in the Coupled Model Intercomparison Project Phase 5 (CMIP5). NorESM1-M is based on the CCSM4 (Gent et al., 2011; Vertenstein et al., 2010) developed at NCAR. NorESM differs from CCSM4 in several aspects. The ocean model POP2 is replaced with a Bergen-developed version of MICOM (Assmann2010, Ottera2010), and the ocean biogeochemistry HAMOCC is coupled to the ocean model. The atmospheric model CAM4 is replaced by CAM4-Oslo (Kirkevåg et al., 2013). As CCSM4, NorESM includes the

ACPD
13, 26389–26450, 2013

Community Land Model (CLM, Oleson et al., 2010) and the Los Alamos Sea Ice Model (CICE). Interface between model components is handled via CPL-7 coupler. The CMIP5 version of NorESM (Bentsen et al., 2013) has been evaluated in terms of climate response and future scenarios (Iversen et al., 2013).

2.2 CAM4-Oslo

The aerosol model in CAM4-Oslo describes the transport and size-resolved aerosol physics and chemistry of 20 aerosol components. The aerosol module combines a life-cycle model which describes the emissions, processing and transport of aerosol mass, to look-up tables calculated by an offline microphysics model. The look-up tables are used to calculate the physical and optical properties of the aerosol population. Aerosols are activated as cloud droplets following Abdul-Razzak and Ghan (2000). A more detailed description of CAM4-Oslo aerosol model can be found in Kirkevåg et al. (2013).

Sea salt emissions produce particles to three different modes: Aitken (median radius $\bar{r} = 22$ nm), accumulation ($\bar{r} = 130$ nm) and coarse ($\bar{r} = 740$ nm). Dust is emitted to accumulation ($\bar{r} = 220$ nm) and coarse modes ($\bar{r} = 630$ nm). Sulfate can condense on all these five modes. Black carbon (BC) is included in five modes of CAM4-Oslo. First, fossil fuel emissions produce two types of BC particles: nucleation-mode size ($\bar{r} = 11.8$ nm) and accumulation-mode size fractal agglomerates ($\bar{r} = 100$ nm). The nucleation-mode BC can become coated with sulfate and moved to an larger, aged BC mode. The black carbon associated with biomass burning is lumped together in an internally mixed mode with organic carbon (OC). In addition to biomass burning emissions, this OC/BC mode is used also for OC emissions from fossil fuels and the production of SOA. The initial radius of the OC/BC mode is 40 nm.

Sulfuric acid produced in the gas phase can either condense on the pre-existing particle distribution or nucleate as new particles. Nucleation mode particles (initial $\bar{r} = 11.8$ nm) can grow to Aitken mode size if not lost by coagulation. Details of nucleation process are presented in Sect. 2.4.1.

ACPD
13, 26389–26450, 2013

2.3 Emissions

The anthropogenic emissions for year 2000 are used in all simulations. The emissions are from the IPCC AR5 dataset (Lamarque et al., 2010). Emissions of sea-salt are modeled interactively as a function of 10 m wind speed and sea-surface temperature according to Struthers et al. (2011), with some updates as described by Kirkevåg et al. (2013). The DMS and dust emissions are prescribed daily values based on AeroCom inventory (Dentener et al., 2006). Volcanic SO_2 emissions are modeled according to the AeroCom emission inventory (Dentener et al., 2006) and distributed evenly throughout the year.

The terrestrial biogenic volatile organic compound (BVOC) emissions of monoterpene and isoprene are considered. The BVOC emissions are prescribed monthly averages calculated with MEGAN2, amounting to 80 Tg (C) yr^{-1} for monoterpene and 530 Tg (C) yr^{-1} for isoprene. We do not include a VOC source over oceans, although oceans are potentially a significant source of VOCs (Shaw et al., 2010). However, NorESM does include a primary organic aerosol source over oceans (Kirkevåg et al., 2013), which is scaled to 8 Tg yr^{-1} as estimated in Spracklen et al. (2011).

Only the BVOC, wildfire, biomass burning, DMS and sea salt emissions in NorESM have seasonal variation. Anthropogenic fossil fuel emissions are annual averages distributed evenly throughout the year. A diurnal emission cycle is only included in the interactive sea salt emission.

2.4 Implemented modifications in NorESM

We have developed NorESM1-M to include an explicit mechanism for nucleation, nuclei growth and SOA formation. The details of the modifications are described below.

ACPD
13, 26389–26450, 2013

2.4.1 Nucleation

The NorESM version in Kirkevåg et al. (2013) includes an implicit mechanism for new particle formation: after condensation, all excess sulfuric acid is assumed to form new particles. Sulfuric acid is not a traced variable. The nucleated particles are placed in the nucleation mode with an initial radius of 11.8 nm.

We have implemented the gaseous sulfuric acid as a prognostic variable, and included a mechanistic description of the nucleation process. Binary homogeneous sulfuric acid-water nucleation is implemented in NorESM according to the parameterization by Vehkamäki et al. (2002). This mechanism is applied throughout the atmosphere, and has been shown to produce a band of particles in the upper troposphere and lower stratosphere (UTLS) (e.g. Makkonen et al., 2009). However, binary homogeneous nucleation can not explain the nucleation events observed in the boundary layer (e.g. Spracklen et al., 2006). For this reason, global aerosol models generally apply either ternary sulfuric acid-ammonia-water nucleation (Pierce and Adams, 2009), ion-induced nucleation (Yu et al., 2008) or a semi-empirical nucleation parameterization (Makkonen et al., 2009) to the model. Ternary nucleation has been shown to perform well in some cases (Gaydos et al., 2005) but generally produce too high number concentrations in the troposphere (Lucas and Akimoto, 2006). Here, we have included activation-type nucleation (Kulmala et al., 2006; Sihto et al., 2006)

$$J_2 = A[H_2SO_4], \quad (1)$$

where the formation rate of 2 nm particles J_2 is a linear function of the sulfuric acid concentration. The activation coefficient $A = 1.7 \times 10^{-6}\ s^{-1}$ is taken from Paasonen et al. (2010). The activation-type nucleation is restricted to the boundary layer.

The nucleated particles are of 1–2 nm diameter. To save computational effort, we do not include the nucleated particles directly in the aerosol model. Instead, we use the parameterisation by Lehtinen et al. (2007) to calculate the formation rate of particles at

ACPD
13, 26389–26450, 2013

the diameter of the nucleation mode.

$$J_x = J_{\mathrm{nuc}} \exp\left(-\gamma \cdot d_{\mathrm{nuc}} \frac{\mathrm{CoagS}(d_{\mathrm{nuc}})}{\mathrm{GR}}\right), \quad (2)$$

where J_x is the formation rate at the nucleation mode size (d_x), J_{nuc} is the nucleation rate of d_{nuc} sized particles, CoagS is the coagulation sink (s^{-1}) and GR is the particle growth rate. The factor γ is a function of d_{nuc} and d_x

$$\gamma = \frac{1}{m+1}\left[\left(\frac{d_x}{d_{\mathrm{nuc}}}\right)^{(m+1)} - 1\right] \quad (3)$$

The exponent m depends on the background aerosol distribution, and could be estimated from coagulation sinks of d_{nuc} and d_x sized particles (Lehtinen et al., 2007). Here we assume $m = -1.6$, which is in the typical range of atmospheric values (Lehtinen et al., 2007).

Coagulation sink CoagS(d_{nuc}) for nuclei is calculated from NorESM aerosol modes. The above formula does not consider intramodal coagulation, which could be important if nucleation rates are extremely high (Anttila et al., 2010). In the case of activation-type nucleation (Eq. 1) we calculate J_x from formation rate of $d_{\mathrm{nuc}} = 2$ nm sized particles, i.e. $J_{\mathrm{nuc}} = J_2$. By default, we convert the nucleation rates to formation rates of 12 nm particles ($J_x = J_{12\,\mathrm{nm}}$) which are then implemented in the nucleation mode of NorESM. The nuclei growth rate GR is calculated from concentrations of sulfuric acid and organic vapours (see Sect. 2.4.3) according to Kerminen and Kulmala (2002).

The greater the difference in sizes d_{nuc} and d_x, the larger values are assigned for m causing the formation rate J_x to be relatively more sensitive to CoagS and GR than to the nucleation rate itself. One sensitivity simulation is made to test the effect of nucleation mode diameter d_x on aerosol number concentration.

ACPD
13, 26389–26450, 2013

2.4.2 SOA formation

In standard NorESM1-M (Kirkevåg et al., 2013) SOA is introduced with a prescribed monthly surface source and the SOA mass is included to the OM/BC mode with assumed initial radii of $\bar{r} = 40$ nm. The SOA formation in NorESM1-M is 37.5 Tg yr^{-1} based on an estimate by Hoyle et al. (2007). Seasonal and temporal variation follow MEGAN2 algorithm. To estimate the particle growth due to organic vapours, we implement an improved SOA scheme in NorESM. Biogenic source for monoterpenes and isoprene is included as prescribed monthly emission fields, pre-calculated by MEGAN2 (Guenther et al., 2006). These SOA precursors are then oxidized in the gas-phase by O_3, OH and NO_3. The formed SOA is assumed to be non-volatile, and no gas-phase tracers are included for the oxidation products. Currently, only monoterpene is assumed to form SOA, with a 15 % yield. It is further assumed that 50 % of the monoterpene ozonolysis products are of enough low volatility that they can partition to the nucleated particles (below 11.8 nm radii) and also participate nucleation itself. This is in accordance with Yli-Juuti et al. (2011) who showed a clear connection with nuclei mode growth and monoterpene ozonolysis. The improved SOA model changes aerosol formation in two ways, by changing the size distribution of formed SOA and by allowing SOA formation outside the surface level of the model.

2.4.3 Growth of nucleated particles

In many locations, the nuclei growth due to organic vapours can clearly exceed the growth by sulfuric acid. For example in Hyytiälä, Finland, sulphuric acid can only explain less than 10 % of particle growth (Riipinen et al., 2011). Experiments in CLOUD have shown that in the presence of organic vapour, organic volume fraction can increase from 0.4 to 0.9 when the particles grow from 2 nm to 63 nm (Keskinen et al., 2013). We assume that organic vapours can grow new particles until they reach nucleation mode. We do not include a tracer for organic mass in the nucleation mode of NorESM: particles entering the aerosol module from nucleation process are assumed to consist

ACPD
13, 26389–26450, 2013

of sulfate. However, the nucleation mode organic mass is very low compared to the total organic aerosol mass.

With the above setup, the modeled growth rates are close to observations. For June, NorESM growth rates in Hyytiälä vary from 1.6 to 4.2 $nm\,h^{-1}$, while the medians of observed June growth rates are 2, 4 and 8 $nm\,h^{-1}$ for size ranges 1.5–3, 3–7 and 7–20 nm, respectively (Yli-Juuti et al., 2011). In Rocky Mountains, US, NorESM simulates a similar range of GR, from 1.0 for 2.6 $nm\,h^{-1}$ (June–July), which is slightly lower than the observed 4 $nm\,h^{-1}$ (Boy et al., 2008). Overall, our approach seems to underpredict particle growth to some extent, possibly due to unaccounted vapours.

The fraction of formed SOA which does not partition to nucleated particles will form SOA the same way as in Kirkevåg et al. (2013): it is lumped together with OC from biomass burning, fossil fuel and marine organic emissions. An initial radius of 40 nm is assumed for the formed SOA. As such, the SOA model in NorESM is improved to take into account its possible role in nucleation and nuclei growth, but the model can not capture the real nature of SOA formation. While the implemented model modifications are likely to improve the simulated effect of SOA formation on particle number, the particle growth after nucleation may be underestimated.

3 Sensitivity experiments

We use NorESM to simulate aerosol number concentrations in a number of sensitivity experiments. The experiments are listed in Table 1 and described in the following sections.

3.1 Black carbon size distribution

The size distribution and the mixing state of BC are strong sources of uncertainty for modeled particle concentrations (Reddington et al., 2011, 2013). Reddington et al. (2013) showed a clear underestimation of BC particle size as well as an overestima-

ACPD
13, 26389–26450, 2013

tion of the number fraction of particles containing a BC core. They suggested that the uncertainties are due to errorneously modeled BC particle mixing state assumptions and too small emission size distribution for a global model scale. Unlike the model in Reddington et al. (2013), NorESM includes two externally mixed modes for fossil fuel BC emission: a nucleation mode of diameter 23.6 nm and a fractal agglomerate mode of diameter 200 nm. A small fraction of 10 % of the BC emission is assumed to be agglomerated particles. The nucleation mode BC size is slightly smaller than the AeroCom recommendation for fossil fuel BC (30 nm), however, the AeroCom recommendation does not include a separate agglomeration mode. The assumed BC diameter is smaller than used by many global aerosol models: 60 nm in Stier et al. (2005) and Zhang et al. (2012), 100 nm in Pierce and Adams (2007).

We address the sensitivity of NorESM aerosol number concentrations to fossil fuel BC emission size by simulations with two emission diameters, 23.6 nm (default for original NorESM1-M) and 47.2 nm. The difference of a factor of 2 in the emission diameter leads to a factor of 8 difference in emitted number of BC particles, which can lead to a notable effect in heavily polluted regions. The difference in BC number concentration will also affect new particle formation: the lower (higher) coagulation sink with larger (smaller) BC particles will act to increase (decrease) the survival of nucleated particles. This is taken into account in the calculation of coagulation sink in Eq. (2).

It should be noted that the applied emission inventory does not include any intra-annual variation for the fossil fuel emissions. This lack of emission seasonality stems from the emission dataset construction and might reduce the correlation between simulated and observed concentrations. Monthly variation of anthropogenic emissions has been included in certain emission datasets (e.g. ECLIPSE, http://eclipse.nilu.no), but are not yet widely used in global aerosol modeling.

3.2 Nucleation

Although many global models tend to use activation-type nucleation by sulfuric acid as the default option, the actual mechanism behind atmospheric nucleation is still unre-

ACPD
13, 26389–26450, 2013

solved. There are indications that organic vapours play a role already in the nucleation process Metzger et al. (2010), and including an organic vapour into the nucleation parameterization might lead to a better correlation with observations (Paasonen et al., 2010). We will test the sensitivity of simulated number concentrations to nucleation rate by an additional simulation with organic nucleation:

$$J_2 = A_{S1}[H_2SO_4] + A_{S2}[ORG] \quad (4)$$

The activation coefficients are 6.1×10^{-7} and $0.39 \times 10^{-7}\,s^{-1}$ for A_{S1} and A_{S2}, respectively (Paasonen et al., 2010). We assume the the organic vapours participating nucleation in Eq. (4) are the same as those involved in nuclei growth, i.e. a 50 % fraction of monoterpene ozonolysis products. Using organic nucleation will change the spatial distribution of particle formation. Also the spatial correlation between particle formation and organics available for particle growth might lead to increased survival of nuclei (Makkonen et al., 2012a).

Additionally, we will run a simulation with nucleation turned off. In this case, the sulfuric acid which would otherwise nucleate, can now condense on the pre-existing particle population, making particle aging more efficient. One additional simulation is performed with a smaller diameter (10 nm) for the nucleation mode (ActNuc_BC24_Nuc10).

3.3 Particle growth

Globally, organic vapours account for a large portion of nuclei growth. With more vapours for growth, more nucleated particles will survive the until the detection limit of CN counter or the nucleation mode of NorESM. We will investigate the role of BVOCs on particle number by simulations without SOA formation. In NorESM, this will effect number concentrations in two ways: decreasing the growth rate in Eq. (2) and the formation of the "primary" OC particles.

ACPD
13, 26389–26450, 2013

3.4 Simulation setup

For all simulations, we use anthropogenic emissions for the year 2000. The sea-surface temperatures are prescribed (AMIP-style run). The model is integrated for 5 yr after one year spin-up. Monthly averages are calculated as multi-year climatological means over 5 simulation years.

We create one experiment to test the sensitivity to modeled meteorology. In all other simulations, the meteorology is unaffected by the CAM4-Oslo aerosols, that is, the meteorology in experiments is identical. However, the simulated climate can be very different from that affecting observed number concentrations. Additionally, the observations at different stations cover different time periods. The experiment ActNuc_BC24_Online couples the radiation, clouds and model meteorology to the CAM4-Oslo aerosols, thereby rendering the meteorology different from other experiments. The changes in meteorology will affect the transport and deposition of aerosols. There is no reason to assume that the meteorology in any of the included simulations would be closer to the real world meteorological state during the aerosol observations, but this approach can provide some estimate of uncertainty.

4 Aerosol observations

4.1 Observations at measurement sites

We compare NorESM aerosol number concentration against observations from 60 surface sites: 51 in the Northern Hemisphere and 9 in the Southern Hemisphere. Where available, we use several years of observations to achieve a representative distribution of aerosol number concentration. As NorESM is not simulated using reanalysed meteorology and emissions of year 2000 are used in all simulations, year-to-year comparisons are not feasible. While some stations are representative for a large surrouding region, some stations are affected by a local aerosol or precursor source. Local effects

ACPD
13, 26389–26450, 2013

(e.g. plumes from power plant) could be filtered out of measurement data to some extent, however we have used all available data from each station. Although NorESM can not reproduce the effects of local pollution, the simulations can provide meaningful information on the background aerosol at the site. The names, locations and altitudes of the stations are listed in Table 4. The aerosol observation data is collected from three databases (EBAS, WDCA and NOAA) and separate publications, as indicated in Table 4.

The experimental setup varies from location to another, and aerosol number concentrations are measured with either Condensation Particle Counters (CPC), Differential or Scanning Mobility Particle Sizers (DMPS/SMPS) or Diffusion Aerosol Spectroscopes (DAS). The lower diameter cutoff ranges from 3 to 15 nm in different stations. Even with 15 nm cutoff diameter the measured particle size range covers basically all aerosol modes in NorESM, as the smallest NorESM modes have a median diameter of 24 nm by default. If particle size distribution information has been available for a station, we have omitted the possible smallest size bins (3–10 nm) from the measured station data. The implemented cutoff diameters are listed in Table 4.

Even with the relatively high number of stations, the spatial coverage of aerosol number concentration observations is rather poor. Most of Europe and parts of North America are rather well represented, while e.g. most of South America and Africa lack long term observations of aerosol number. To make up for the unavailability of long-term data sets, we use campaign data to fill some of the spatial gaps.

4.2 Vertical observations

To complement the limitations of spatially fixed site observations, we use airborne measurements to evaluate the vertical distribution of NorESM aerosol concentrations. The flight campaign data is extracted from a compilation by Clarke and Kapustin (2010), which includes flight campaigns along Asian coastlines (ACE-Asia, TRACEP), South Pacific (ACE-1, PEMT-A, PEMT-B), North Pacific (INTEX-B Hawaii, INTEX-B Alaska), Arctic (ARCTAS) and North America (IMPEX, INTEX-A, INTEX-B Houston). The obser-

ACPD
13, 26389–26450, 2013

vation cutoff diameter was 12–14 nm in ACE-Asia and PEMT-A, and 8–12 nm in other campaigns. The monthly average simulated fields are sampled over the regions indicated in Clarke and Kapustin (2010) and Fig. 4, hence the footprint of vertical profiles is not identical in simulations and measurements.

4.3 Marine boundary layer

To study aerosol number concentrations over oceans, we evaluate NorESM against the data compiled by Heintzenberg et al. (2000). The dataset covers all major ocean regions, including data from both remote ocean and coastal sites. However, the dataset does not include concentrations from the North-Western Pacific, which is a major contributor to particle concentrations in NorESM. We mask out coastal regions (Supplement Fig. S1) in NorESM and focus on remote ocean regions.

5 Results and discussion

5.1 General features of simulated number concentrations and responses to perturbations

Figure 1 shows a map of annual-mean (5 yr average) ground level aerosol number concentration from a simulation with activation-type nucleation and small BC particles (ActNuc_BC12). Highest concentrations are found in Asia, peaking at 10 000–50 000 cm^{-3}. Most land areas are covered by concentrations above 1000^{-3}, while pristine regions in Greenland and Antarctica reach concentrations as low as 100 and 10 cm^{-3}, respectively. The land-ocean contrast (Table 2) is about three-fold, with averages of 2200 cm^{-3} over land areas and 400 cm^{-3} over ocean areas.

The four panels in Fig. 2 show the sensitivity of aerosol number to nucleation, SOA formation, BC emission size, and nucleation parameterization.

Nucleation is relatively least effective in the high wind-speed band around 60S (Fig. 2a), which is dominated by sea salt particles. Otherwise, nucleation increases

ACPD
13, 26389–26450, 2013

aerosol number concentration over oceans by more than 20 % in large areas. Some continental regions with high primary emissions, such as Asia, show a small sensitivity of > 5 % to nucleation. In most cases, the increase in aerosol number due to nucleation is more than 20 %, or even 50 % in North America. The sensitivity of aerosol number concentration to nucleation in a certain area is a combination of background particle sink and available vapours (sulfuric acid and organics). If the background sink is lowered, relative importance of nucleation increases. This can be shown comparing simulations ActNuc_BC12 and ActNuc_BC24 with their respective _NoNuc counterparts: with a lower sink, nucleation increases continental aerosol number concentration by 90 % (ActNuc_BC24 vs. NoNuc_BC24), while a higher background sink shows a lower sensitivity of 50 % to nucleation (ActNuc_BC12 vs. NoNuc_BC12). If SOA formation is turned off, the sensitivity is further suppressed to 40 % (ActNuc_BC12_NoSOA vs. NoNuc_BC12_NoSOA), illustrating the importance of organic vapours.

Turning on nucleation increases global average number concentration by 561 cm^{-3} with larger BC particles (24 nm), but only by 471 cm^{-3} with smaller BC particles due to increased coagulation sink. Decreasing the SO_4 nucleation mode diameter to 10 nm in the model almost doubles the simulated global number concentrations.

In many areas, the organics make a significant contribution to the increased survival of nucleated particles until they reach the nucleation mode size in NorESM. This increases the sensitivity of aerosol number concentrations to SOA formation. Since we have not implemented SOA precursor emissions over oceans, the land-ocean contrast of SOA sensitivity is large (Fig. 2b). Only westerly outflow from South America shows increases over 5 %.

Varying the emission radius of fossil fuel BC particles between 12 and 24 nm leads to a variation of around 20 % in Europe and Asia (Fig. 2c). The effect of changes in BC size is generally confined to areas near continental emission sources, although some signal can be seen in the main shipping routes in the North Atlantic and Pacific Ocean.

Although the global aerosol number concentration is not sensitive to the choice of nucleation parameterization (5 %, Table 2), Fig. 2d shows interesting spatial differences

ACPD
13, 26389–26450, 2013

from ActNuc_BC12 and OrgNuc_BC12 simulations. In areas with strong biogenic VOC emissions, organic nucleation (OrgNuc_BC12) can lead to 5–50 % higher concentrations, even > 50 % over South America, compared to ActNuc_BC12. In areas dominated by anthropogenic emissions, activation-type nucleation (ActNuc_BC12) leads roughly to 5 % higher concentrations than organic nucleation.

5.2 Comparison to site observations

Figure 3 shows the locations of the 60 sites used in the analysis. We will investigate the performance of NorESM with respect to number concentration bias, defined as the difference between simulated and observed monthly average aerosol number concentration. We also calculate the correlation coefficients R^2 between the simulated and observed monthly mean concentrations to evaluate the simulated intra-annual variation of concentrations. The colour code of each station in Fig. 3 indicates the number concentration bias in simulation ActNuc_BC24 (blue: bias < −20 %, red: bias > +20 %). The contours in the background show simulated aerosol number concentrations from the ActNuc_BC24 experiment.

The stations are divided into 6 groups. First, we separate stations in the Arctic (Pallas, Värriö, Zeppelin and Point Barrow) and Antarctic (Dome C, South Pole, Troll and Neumayer). Next, we group stations located at high altitude (1000 m a.s.l.). However, some high altitude stations belong to other groups based on their location or representativeness. Finally, we group remaining stations stations as marine, remote or rural. We use the classifications in Spracklen et al. (2010) and Henne et al. (2010) as guidance. While some stations are representative of a rather homogenous region, some stations might exhibit diverse concentrations depending on e.g. wind direction.

5.2.1 Arctic sites

The comparison against Arctic sites is shown in Fig. 5. The simulations can capture the seasonal variation in the Arctic with correlation coefficients ranging from $R^2 = 0.25$

ACPD
13, 26389–26450, 2013

without nucleation to $R^2 = 0.51$ with nucleation included. The Arctic sites Barrow and Zeppelin show very similar observed number concentration pattern with annual maximum (minimum) in July (October). Although Pallas and Värriö are high latitude sites, they are heavily influenced by terrestrial biogenic emissions: when turning SOA production off in the model, the number concentrations decrease to the same level as in simulations without nucleation. The model simulations including nucleation and SOA formation overestimate the summer number concentrations in Pallas and Värriö, perhaps indicating too high sensitivity of new particle formation to organic vapours. On the other hand, simulations without nucleation or SOA formation underestimate the concentrations and magnitude of the seasonal cycle. In Barrow, two distinct concentration peaks are seen in April–May and August in the model simulations, and to a lesser extent in the observations. The concentrations at Zeppelin are well reproduced, although winter concentrations are somewhat overestimated. The aerosol concentrations in the Arctic are sensitive to transport, and the simulation ActNuc_BC24_Online with different meteorology seems to work best with $R^2 = 0.62$ and bias of +22 %, mostly due to differences in Point Barrow and Zeppelin stations.

5.2.2 Marine sites

NorESM has difficulties in simulating the number concentrations in marine areas (Fig. 8), where R^2 varies between 0.09 and 0.17. NorESM includes a natural primary organic aerosol marine source (Kirkevåg et al., 2013), which is missing in many global aerosol models. However, marine VOC emissions are neglected. In the NorESM version used in this study, the DMS emissions are prescribed daily fields for each grid box, hence they are not affected by model meteorology.

The model fails to simulate the concentration variation in Mace Head and Cape Grim: in both locations, NorESM clearly overestimates the concentrations in the summer and underestimates in the winter. However, the observations in Mace Head and Cape Grim are highly variable, with even a factor of 3–4 between observed monthly mean and

ACPD
13, 26389–26450, 2013

median concentrations. The coastal areas in Mace Head are a source of iodine compounds, which have been suggested as precursors for nucleation (O'Dowd and Hoffmann, 2005). These iodine nucleation events are not included in the model, which can account for a large fraction of the discrepancy between NorESM and observations. In Cape Grim, the simulations without nucleation correlate well with the observed monthly median values, but all model experiments fail to reproduce the mean concentrations. The model also has trouble reproducing the relatively constant concentrations in Trinidad Head, where the overestimation of intra-annual variation is largely due to SOA: the _NoSOA experiments are almost identical to simulations without nucleation.

The number concentrations at Samoa, Sable Island and Cape Point are rather well simulated, if nucleation is included in the model. In marine sites, switching on nucleation turns the negative bias of −53 to −31 % (no nucleation) to a positive bias of 25–39 % (nucleation on). With the exception of Sable Island, the seasonal cycle is not improved by including either nucleation or SOA formation in the simulation. During January–May, nucleation is needed to explain concentrations in Cape San Juan, however nucleation overestimates concentrations during the rest of the year.

5.2.3 High altitude sites

From the six categories in this study, the model performance in high altitude sites (Fig. 7) is second-best in terms of monthly correlations. The correlations averaged over all 14 sites range from 0.39 to 0.51. While simulations without nucleation clearly underestimate concentrations, including nucleation improves model bias and increases correlation coefficient R^2 from 0.39–0.40 to 0.50–0.51 (ActNuc_BC12 and ActNuc_BC24).

The model strongly exaggerates the intra-annual variation in Storm Peak Laboratory site, while the model can only explain about 10 % of the wintertime concentrations. The Storm Peak measurement station is located very close to the Niwot Ridge station. In Niwot Ridge, the ActNuc_BC24 simulation reproduces the observed concentrations very well, although the observation station was heavily influenced by local pollution from lower elevations. In many high-altitude sites the annual average concentrations

ACPD
13, 26389–26450, 2013

are well reproduced, but the rise in number concentrations in early spring is usually underestimated (Jungfraujoch, Puy de Dome, Zugspitze, Moussala, Mount Washington, Mount Cimone). The only South American station in this evaluation is located in Pico Espejo, where the seasonality is extremely well reproduced ($R^2 = 0.47$ for ActNuc_BC24_Nuc10), but the concentrations are generally slightly underestimated.

There is a strong contrast between model and observations in Mauna Loa: simulations indicate very high concentrations, mainly from nucleation (even > 90 %), whereas the observations show very little intra-annual variation and low concentrations. The SO_2 emissions from Mauna Loa volcano have been reported declining, falling under detection limits by the year 2000. However, the volcanic emissions in NorESM, based on AeroCom, show high SO_2 emission from the Kilauea volcano. Also, Mauna Loa stations is located near 4000 m altitude, and NorESM shows strong transport from Western US towards Mauna Loa during the summer (see comparison to INTEX-B Hawaii in Sect. 5.4).

5.2.4 Antarctic sites

The Antarctic aerosol loading is affected by natural emissions of sea salt and DMS as well as long-range transport of dust and anthropogenic pollution (Kyrö et al., 2013). Local and regional new particle formation can also increase number concentrations in the Antarctic (Kyrö et al., 2013). The simulated number concentrations in the Antarctic (Fig. 6) are rather insensitive to the performed model parameter perturbations, although the simulations with original NorESM1-M setup and experiment ActNuc_BC24_Nucl10 are somewhat separated due to strong nucleation in summer. All simulations show very high correlation with observations, with R^2 ranging from 0.76 to 0.88 (excluding ActNuc_BC24_Nuc10). Except for the South Pole site, the summer concentrations are generally underestimated. The extremely low observed winter concentrations of few tens to 100 cm^{-3} are well reproduced by NorESM.

ACPD
13, 26389–26450, 2013

5.2.5 Remote sites

The summer minimum, observed during July–August in Birkenes, Aspvreten, Hyytiälä and Vavihill, is not reproduced in the model simulations (see Fig. 9). The neighbouring stations Listvyanka and Tomsk seem similar in model results, while the simulated wildfire event in May is observed only in Tomsk. In all stations except Listvyanka and Preila, the observed winter concentrations are well captured by the model. However, the summer concentrations are generally overestimated (underestimated) by simulations with (without) nucleation. Since the seasonal cycle is generally overestimated in simulations with nucleation, turning off SOA formation actually improves the correlation coefficient (from $R^2 = 0.38$ to $R^2 = 0.48$–0.53). Still, simulations without SOA formation underestimate overall concentrations with a bias of −17 to −41 %.

5.2.6 Rural sites

With the high anthropogenic emissions in the rural sites, the model performance is highly sensitive to the selected model parameters. The R^2 ranges from 0.21 with NoNuc_BC12 to 0.38 with ActNuc_BC24 and the bias ranges from a clear underestimation of −69 % with NoNuc_BC24 to +31 % with ActNuc_BC24_Nuc10. Although improving model bias, decreasing the BC emission size from 24 to 12 nm decreases the correlation coefficient from 0.38 to 0.34 and from 0.31 to 0.18 with and without nucleation, respectively. The original NorESM1-M has a bias of +20 %, and including a mechanistic model for new particle formation can significantly improve the modeled seasonal cycle. Also, disabling SOA formation in the model degrades the simulated seasonal cycle.

NorESM can clearly not reproduce the high concentrations in Po Valley or Ispra during wintertime partly due to difficulties in simulating the boundary layer structure and topography with the coarse spatial resolution of NorESM. Although NorESM can capture the transport of pollutants from Northern Africa to Izaña, the local sources (vehicles, ships) dominate the observed number concentrations at the urban site (Gonzàlez et al.,

ACPD
13, 26389–26450, 2013

2011). The concentrations at the Indian Himalayan station are well simulated without nucleation (NoNuc_BC24: $R^2 = 0.62$). Turning on nucleation (ActNuc_BC24) does not improve the correlation between measurements, but leads to a slight overestimation. The location is very much affected by local emissions in the simulations: decreasing BC emission size to 12 nm increases the simulated number concentrations by as much as a factor of 4.

5.2.7 Global scale analysis

Mean (median) correlation coefficients (Table 3) of monthly averages calculated over all stations range from 0.30 (0.23) in NoNuc_BC12 to 0.42 (0.50) in ActNuc_BC24_NoSOA. The online-meteorology simulation ActNuc_BC24_Online (median $R^2 = 0.46$) performs somewhat better than the offline-version ActNuc_BC24 (median $R^2 = 0.43$), which could indicate that the meteorology (transport, deposition) in the online-simulations is on average closer to the actual meteorology during observations. Averaged over all stations, larger fossil fuel BC particles (BC24) result in better correlation than the smaller 12 nm particles. Without nucleation, the mean (median) correlation is increased from 0.30 (0.23) to 0.35 (0.31) when doubling the BC emission size (NoNuc_BC12 vs. NoNuc_BC24). With nucleation turned on in the model, the respective mean (median) correlation coefficient increases from 0.40 (0.39) to 0.41 (0.43) due to doubling of BC emission size. Again, it is important to remember that the anthropogenic emissions, such as fossil fuel BC, do not include an intra-annual cycle, which can affect the resulting correlation. Although Fig. 2 shows strong effect from nucleation itself, the performance of activation-type and organic nucleation are rather similar, resulting in a bias of +20 % and correlation coefficients of 0.39 (OrgNuc_BC12) and 0.40 (ActNuc_BC12).

Simulations without nucleation lead to a low bias of −64 % and −27 % and the smallest correlation coefficients of 0.35 and 0.30 for NoNuc_BC24 and NoNuc_BC12, respectively. Turning on nucleation in the simulations reduces the bias to −5 % and +20 % and increases the correlation coefficient to 0.41 and 0.40 for ActNuc_BC24

ACPD
13, 26389–26450, 2013

and ActNuc_BC12, respectively. Averaged over all stations, SOA formation does not have a large effect on the seasonal cycle: the mean (median) R^2 is 0.42 (0.42) and 0.41 (0.43) with ActNuc_BC24_NoSOA and ActNuc_BC24, respectively. However with large BC emission size, simulations without SOA formation clearly underestimate the observed number concentrations.

Although the mean bias of +33 % for the original NorESM1-M setup indicates clear overestimation of aerosol number, the amount of stations with a bias between −30 % and +30 % is almost identical (28–29) in NorESM1-M, OrgNuc_BC12, ActNuc_BC12 and ActNuc_BC24. On the other hand, the median bias calculated over all 10 experiments exceeds +30 % in 12 stations and is below −30 % in 21 stations. While there are more stations where NorESM underestimates aerosol number concentrations, the overestimations on certain stations are considerable. Averaging over all stations in Northern Hemisphere, all model experiments generally underestimate aerosol number concentrations during October–May and overestimate in the summer time.

There are several stations where the correlation between observed and measured monthly averages is poor ($R^2 < 0.1$): Botsalano, Marikana, Mace Head, Cape Grim, K-Puszta, Trinidad Head and Lulin. In all of these stations except Trinidad Head and Marikana, the R^2 also varies less than 0.07 between experiments. It is clear that the performed simulations and sensitivity experiments can not capture the uncertainties related to the discrepancy between model and observations. On the other hand, there are locations where the R^2 varies more than 0.5 between simulations: Indian Himalaya, Bondville, Sable Island, Utö and Thompson Farm.

5.3 Campaign observations

Langley et al. (2010) presented aerosol number and CCN concentrations from ship cruise in North Pacific Ocean. The average aerosol number concentration observed between 9 and 27 July 2002 was 500 cm^{-3}, which is close to the July average of 575 cm^{-3} found in the ActNuc_BC24 simulation.

ACPD
13, 26389–26450, 2013

Rissler et al. (2006) investigated results from the LBA-SMOCC campaign in Amazon, Brazil. Total aerosol number concentrations of 11 440 ± 6790, 5550 ± 3170 and 2070 ± 1790 cm^3 were found for dry (11 September–8 October), transition (9 October–30 October) and wet season (31 October–14 November), respectively. The corresponding simulated concentrations from the ActNuc_BC24 simulation are 24 000, 6000 and 2600 cm^3. Although the dry season number concentration is overestimated by the model, the transition to wet season is well reproduced.

5.4 Vertical observations

The vertical aerosol number concentrations profiles are compared against Clarke and Kapustin (2010) in Fig. 11. The comparison covers 12 flight campaigns over Asia, Pacific Ocean, Arctic, North America and Atlantic. The areas are shown in Fig. 4.

In Asian (ACE-Asia, TRACE-P) and North American (INTEX-A) outflow regions the shape of the vertical profile and the number concentrations are well simulated, with a steep gradient between the surface and 3 km altitude. Even with a factor of 3 difference in simulated concentrations, NorESM underestimates the observed high concentrations below 1 km altitude in TRACE-P and INTEX-A. In ACE-Asia, including nucleation or using small BC particle size leads to a slight overestimation of particle number above 3 km. In TRACE-P and INTEX-A, the simulations are generally in the uncertainty range of observations. In these three regions, the observed increase in concentrations with altitude above 4–5 km is successfully simulated only for INTEX-A, and to some extent for TRACE-P in simulations with smaller diameter for nucleated particles (ActNuc_BC24_Nuc10).

The observed gradient between 3 and 6 km in ACE-1 is reproduced by NorESM, even though the concentrations are generally underestimated. The simulated low-level concentrations are greatly affected by continental Australian emissions, which are not sampled during ACE-1 flights. NorESM fails to reproduce the steep gradient in the free troposphere over the Pacific Ocean (PEMT-A and PEMT-B), where observations show aerosol concentrations increasing by a factor of 2–5 between

ACPD
13, 26389–26450, 2013

1 km and 8 km. Only the experiment with increased sensitivity to nucleation (ActNuc_BC24_Nuc10) shows some increase in concentration with altitude above 4 km. However, ActNuc_BC24_Nuc10 clearly overestimates concentrations below 3 km in PEMT-B. The simulated peak between 1–2 km in PEMT-A originates from South American OC emissions and is not visible in averaged observed concentrations, however, the observed variation in PEMT-A is large (Clarke and Kapustin, 2010). North of PEMT-A and PEMT-B, the region of INTEX-B Hawaii receives significant concentrations via long-range transport from both Asia and North America, which is visible also in Fig. 1. Even though the amount of observed profiles in INTEX-B Hawaii is the lowest of Clarke and Kapustin (2010), the concentrations around Hawaii are rather well simulated.

Further north over the Pacific Ocean are the INTEX-B Alaska and more continentally influenced IMPEX profiles. Observations in both INTEX-B Alaska and IMPEX show a steep gradient between surface and 3–6 km altitude. Although simulations are in the uncertainty range of observations, NorESM has difficulty in reproducing the observed profile in either region. In IMPEX, nucleation and SOA formation increase particle number concentrations at 0–2 km altitude by even 250 % and 50 %, respectively, but the model still underestimates the observed concentrations. In both INTEX-B and IMPEX, decreased nucleation mode size (ActNuc_BC24_Nuc10) increases number concentrations below 2 km, but the model still likely underestimates surface sources. In INTEX-B Alaska, the simulated profile is dominated by long-range transport from Asia and is almost the opposite of the observed profile. The ARCTAS campaing region is located just north from INTEX-B Alaska. NorESM simulates rather well the observed concentrations increasing with altitude in ARCTAS, although all experiments likely underestimate the observed concentrations. The original NorESM1-M performs best in terms of concentration gradient and absolute concentrations. The study region of ARCTAS contains the Barrow station, which shows concentrations of 170 and 240 cm^{-3} in March and April, respectively (Fig. 5). The March concentration in Barrow is well simulated by NorESM, but the April concentration is overestimated by the NorESM1-M simulation.

ACPD
13, 26389–26450, 2013

The MIRAGE and INTEX-B Houston observations cover a similar area around Mexico, and show high concentrations (e.g. from Mexico City) near surface as well as above 2 km altitude. The model shows high concentrations near surface (over 4000 cm^{-3}), but is still underestimating the observed values. Only the original NorESM1-M can reproduce the observed maxima around 3–4 km to some extent. It should be kept in mind that the NorESM profiles are monthly averages.

Overall, most simulations produce similar shape of vertical profiles for the cases studied here. 80 % of the simulated concentrations are within one standard deviation of measured concentrations, however, the model is generally biased low. Nucleation is relatively efficient in increasing number concentrations near surface (below 2 km) and in the upper troposphere. Nucleation can increase concentrations near surface by a factor of 5 in INTEX-A, MIRAGE and INTEX-B Houston (ActNuc_BC24 vs. NoNuc_BC24). The increase in number concentration due to nucleation at 8 km altitude ranges from +50 % in INTEX-B Hawaii and ACE-Asia to +400 % in INTEX-A.

The sensitivity simulations for the assumption of BC particle size apply only to fossil fuel emission diameter. Hence, the effect of BC particle size is large close to surface near emission sources and higher up in the atmosphere of main transport regions. Indeed, decreasing the BC particle size from 24 nm to 12 nm (ActNuc_BC12 vs. ActNuc_BC24) increases the near-surface (0–1 km) particle number concentrations by 100 % in ACE-Asia and TRACE-P. Transported BC particles are important in ARCTAS, INTEX-B Hawaii and INTEX-B Alaska, where the decrease in BC particle size increases number concentrations by 25 % (at 5 km), 30 % (at 2 km) and 25 % (at 4 km), respectively. In other regions, the effect of BC size is rather insignificant.

With the current implementation of SOA formation mechanism, the effect of SOA on number concentrations in Fig. 11 is generally below 50 %. With SOA precursor emissions in a region with significant nucleation, the organic vapours can greatly increase particle survival rates. Figure 2 shows rather high sensitivity of number concentration to SOA formation in the region of ARCTAS. However, the ARCTAS campaign was conducted in March–April, when the BVOC emissions are rather low. The effect of SOA

ACPD
13, 26389–26450, 2013

formation on is 15–30 % below 1 km in ARCTAS, 5–8 % between 2–8 km. Due to transport from South America to the region of PEMT-B, the effect of SOA can be seen increasing with altitude, reaching a maximum of 15 % at 8 km.

5.5 Number concentration over oceans

Figure 12 shows the comparison of remote ocean number concentrations from NorESM against the dataset compiled by Heintzenberg et al. (2000). Even over remote ocean areas, the simulated concentrations are very sensitive to nucleation and BC size. SOA formation has no virtually impact in simulations without nucleation, but in simulations with nucleation the SOA formation increases number concentrations by 15–20 %.

All simulations fail to match even the observed uncertainty range between 40° S–20° S, which could be due to coastal influence in the observations (South Africa, Australia). Also the concentrations near Antarctic are somewhat low compared to observations, which was also observed in the Neumayer and Troll stations.

6 Conclusions

The Norwegian Earth System Model, NorESM1-M, was evaluated against atmospheric observations of aerosol number concentration. The measurement data consisted of 63 stations with varying data amounts, flight observation campaigns, individual measurement campaigns and a compilation of marine aerosol concentrations. The observed monthly average number concentrations ranged from 10 cm^{-3} near the South Pole to over 10 000 cm^{-3} in polluted environments.

The aerosol module in NorESM1-M was further developed to improve the representation of atmospheric nucleation and SOA formation. Evaluating NorESM against site observations revealed information on the relative importance of several processes contributing to aerosol number concentrations. Simulations with nucleation switched

ACPD
13, 26389–26450, 2013

off showed a large negative bias (−64 %, NoNuc_BC24). The bias can be reduced (to −26 %, NoNuc_BC12) by adjusting the size of emitted fossil fuel BC primary diameter from 24 nm to 12 nm. However, this adjustment degrades the simulated seasonal cycle (R^2 decreases from 0.34 to 0.29). Introducing explicit nucleation parameterizations in the model improves both seasonal cycle (R^2 = 0.40–0.42) and model bias (to −5–21 %). Although generally overestimating observed concentrations (bias = +33 %), the aerosol microphysics in the original NorESM1-M reproduced the seasonal cycle rather well (R^2 = 0.37).

Considering the difficulties in modeling the dynamics of aerosol population in a global climate model, the NorESM performs well compared to several other models (Spracklen et al., 2010; Makkonen et al., 2012a) with global median correlation coefficient of R^2 = 0.40 and bias = −6 % in the ActNuc_BC24 simulation. Coupling aerosols to model physics affected the meteorology, resulting in somewhat improved results (R^2 = 0.42). However, the model has clear difficulties in modeling number concentrations in certain locations. A dominant problem of the model is overestimation of the seasonal variation over continents, which is possibly both due to overestimated sensitivity to biogenic emissions and underestimated sink for condensing vapours and small nuclei.

Comparison to vertical observations showed that NorESM can reproduce the vertical profiles in continental outflow regions and in the Arctic, but concentrations near pollution sources or in the free troposphere over the remote Pacific Ocean are not well captured. A more detailed study on simulated vertical profiles is under preparation.

There are several limitations in the evaluation approach which prevent a detailed quantitative validation of model performance. The atmospheric model in NorESM can not be nudged against observed reanalysis meteorology, hence the simulated meteorology can be substantially different from the real meteorology during the available observations. To approach this problem we performed a sensitivity simulation with a different meteorology, however this can only provide a limited estimate of uncertainty from

ACPD
13, 26389–26450, 2013

model meteorology. In order to minimize the effect of meteorology, we have averaged the aerosol observation data over several year where available.

The spatial resolution of the model poses a problem when comparing to point-observations: the model grid boxes are 210 km × 280 km at the Equator. The model can therefore not take into account e.g. complex topography around measurement sites. Also, the 60 stations included in the study present varying degree of spatial footprint: some stations are strongly influenced by local point-sources, while others are surrounded by rather homogenous environment. Some of the local source effects could be removed by e.g. filtering out aerosol observation from certain wind sectors, which was not accounted for in this study.

One inherent model deficiency is the lack of intra-annual variation in the anthropogenic aerosol and precursor emissions in most global emission inventories (e.g. AeroCom). which could have a significant effect on aerosol number concentrations on some of the studied stations. The applied emissions are for the year 2000, and might not adequately represent the actual emissions during the observations.

Althought the study was able to utilize aerosol observation data from 60 stations with varying amount of data, the role of long-term aerosol measurements for model evaluation remains critical. In many cases a point-by-point comparison between a global aerosol model and observation is not feasible, which limits the applicability of campaign data for model evaluation. Also, the airborne observations of aerosol vertical profiles are extremely useful when analyzing the overall performance of model transport coupled with aerosol microphysics.

Supplementary material related to this article is available online at http://www.atmos-chem-phys-discuss.net/13/26389/2013/acpd-13-26389-2013-supplement.pdf.

Acknowledgements. R. M. acknowledges CRAICC for financial support. The authors wish to thank the CRAICC project for facilitating the co-operation leading to this article. The work by

ACPD
13, 26389–26450, 2013

T. I., A. K., Ø. S. and J. E. K. has been supported by the Research Council of Norway through the NorClim, EarthClim (207711/E10) and NOTUR/NorStore projects and by the Norwegian Space Centre through PM-VRAE. Additionally, T. I., A. K., and Ø. S. acknowledge support through the EU projects PEGASOS and ACCESS. This study was supported by the Norwegian Research Council's Programme for Supercomputing (NOTUR) through a grant of computing time. We are grateful to NCAR and the development teams for CCSM4 and CESM1 for access to their model code. Technical assistance on NorESM from Kari Alterskjær is acknowledged.

The authors wish to acknowledge the EBAS (http://ebas.nilu.no), NOAA (ftp://ftp.cmdl.noaa.gov/aerosol), WDCA (http://www.gaw-wdca.org) databases, and especially the individual institutions for submitting aerosol data to these databases. Below are acknowledgements for each station that provided data to this study through the above databases:

Mount Cimone: Angela Marinoni and Paolo Bonasoni, Institute of Atmospheric Sciences and Climate of the Italian National Research Council, Italy

Bösel, Hohenpeissenberg, Schauinsland, Waldhof, Zugspitze: Wolfram Birmili, Leibniz Institute for Tropospheric Research, Germany

Troll: Chris Lunder, Norwegian Institute for Air Research, Norway

Cape Point: Casper Labuschagne, South African weather service, South Africa

Storm Peak: Gannet Hallar, Desert Research Institute, USA

Mace Head: Colin O'Dowd, Department of Experimental Physics, National University of Ireland

Moussala: Christo Angelov, Institute for Nuclear Research and Nuclear Energy, Bulgaria

Ispra: Jean-Philippe Putaud, Joint Research Centre, Italy

Zeppelin: Johan Ström, Stockholm University, Sweden

Barrow, Bondville, Mauna Loa, Sable, Samoa, SGP, South Pole, Trinidad Head, Niwot Ridge: John A. Ogren, National Oceanic and Atmospheric Administration, USA

Cape Grim: John Gras, CSIRO Atmospheric Research, Australia. The Cape Grim Program and Global Atmospheric Watch are acknowledged.

Puy de Dôme: Karine Sellegri, National Center for Scientific Research, France. Observatoire de Physique du Globe (OPGC) is acknowledged.

Cabauw: Moerman Marcel, Netherlands Organisation for Applied Scientific Research

Hyytiälä, Pallas: Markku Kulmala, University of Helsinki, Finland

ACPD
13, 26389–26450, 2013

K-Puszta: Markku Kulmala, University of Helsinki, Finland. Hungarian Meteorological Service is acknowledged.
Birkenes: Markus Fiebig, Norwegian Institute for Air Research
Finokalia: Nikos Mihalopoulos, University of Crete, Greece
Vavihill: Erik Swietlicki, Lund University, Sweden
Cape San Juan: Olga L. Mayol-Bracero, University of Puerto Rico – Rio Piedras
Harwell: Roy Harrison, University of Birmingham, UK
Neumayer: Rolf Weller, Alfred Wegener Institute, Germany
Izaña: Rodriguez Sergio, Agencia Estatal de Meteorologia, Izana Atmospheric Research Center, Spain
Boone: James Sherman, Appalachian State University, USA
Preila: Vidmantas Ulevicius, Center for Physical Sciences and Technology, Lithuania
Jungfraujoch: Urs Baltensperger, Paul Sherrer Institute, Switzerland
Montseny: Andrés Alastuey, Institute of Environmental Assessment and Water Research, Consejo Superior de Investigaciones Científicas, Barcelona, Spain
Kosetice: Zdimal Vladimir, Institute of Chemical Process Fundamentals, Czech Republic
Lulin: Neng-Huei Lin, National Central University, Taiwan, Taiwan EPA is acknowledged.
German Federal Environment Agency (UBA), and the German Ultrafine Aerosol Network (GUAN) are acknowledged.
Measurements at Bösel, Waldhof, Schauinsland, and Zugspitze were supported by the German Federal Environment Ministry (BMU) grant F&E 370343200 (German title: "Erfassung der Zahl feiner und ultrafeiner Partikel in der Außenluft"), 2008–2010.
This work was carried out with the support of the FP6 European Commission project European Supersites for Atmospheric Aerosol Research, EUSAAR, contract No. RII3-CT-2006-026140, the European Seventh Framework Program, "ACTRIS, Aerosols, Clouds, and Trace gases Research Infra Structure Network."

References

Abdul-Razzak, H. and Ghan, S. J.: A parameterization of aerosol activation 2. Multiple aerosol types, J. Geophys. Res., 105, 6837–6844, 2000. 26393

ACPD
13, 26389–26450, 2013

Adams, P. and Seinfeld, J.: Predicting global aerosol size distributions in general circulation models, J. Geophys. Res.-Atmos., 107, 4-1–4-23, doi:10.1097/00132985-200204000-00004, 2002. 26391

Allan, J., Bower, K., Coe, H., Boudries, H., Jayne, J., Canagaratna, M., Millet, D., Goldstein, A., Quinn, P., Weber, R., and Worsnop, D.: Submicron aerosol composition at Trinidad Head, California, during ITCT 2K2: its relationship with gas phase volatile organic carbon and assessment of instrument performance, J. Geophys. Res., 109, D23S24, doi:10.1029/2003JD004208, 2004. 26438

Amundsen, C., Hanssen, J., Semb, A., and Steinnes, E.: Long-range atmospheric transport of trace elements to southern Norway, Atmos. Environ., 26A, 1309–1324, 1992. 26437

Anenberg, S., Schwartz, J., Shindell, D., Amann, M., Faluvegi, G., Klimont, Z., Janssens-Maenhout, G., Pozzoli, L., van Dingenen, R., Vignati, E., Emberson, L., Muller, N., Jason West, J., Williams, M., Demkine, V., Kevin Hicks, W., Kuylenstierna, J., Raes, F., and Ramanathan, V.: Global air quality and health co-benefits of mitigating near-term climate change through methane and black carbon emission controls, Environ. Health Persp., 120, 831–839, doi:10.1289/ehp.1104301, 2012. 26390

Anttila, T., Kerminen, V.-M., and Lehtinen, K.: Parameterizing the formation rate of new particles: the effect of nuclei self-coagulation, J. Aerosol Sci., 41, 621–636, doi:10.1016/j.jaerosci.2010.04.008, 2010. 26396

Asmi, A., Wiedensohler, A., Laj, P., Fjaeraa, A.-M., Sellegri, K., Birmili, W., Weingartner, E., Baltensperger, U., Zdimal, V., Zikova, N., Putaud, J.-P., Marinoni, A., Tunved, P., Hansson, H.-C., Fiebig, M., Kivekäs, N., Lihavainen, H., Asmi, E., Ulevicius, V., Aalto, P. P., Swietlicki, E., Kristensson, A., Mihalopoulos, N., Kalivitis, N., Kalapov, I., Kiss, G., de Leeuw, G., Henzing, B., Harrison, R. M., Beddows, D., O'Dowd, C., Jennings, S. G., Flentje, H., Weinhold, K., Meinhardt, F., Ries, L., and Kulmala, M.: Number size distributions and seasonality of submicron particles in Europe 2008–2009, Atmos. Chem. Phys., 11, 5505–5538, doi:10.5194/acp-11-5505-2011, 2011. 26437

Bentsen, M., Bethke, I., Debernard, J. B., Iversen, T., Kirkevåg, A., Seland, Ø., Drange, H., Roelandt, C., Seierstad, I. A., Hoose, C., and Kristjánsson, J. E.: The Norwegian Earth System Model, NorESM1-M – Part 1: Description and basic evaluation of the physical climate, Geosci. Model Dev., 6, 687–720, doi:10.5194/gmd-6-687-2013, 2013. 26393

Birmili, W., Berresheim, H., Plass-Dülmer, C., Elste, T., Gilge, S., Wiedensohler, A., and Uhrner, U.: The Hohenpeissenberg aerosol formation experiment (HAFEX): a long-term

ACPD
13, 26389–26450, 2013

study including size-resolved aerosol, H_2SO_4, OH, and monoterpenes measurements, Atmos. Chem. Phys., 3, 361–376, doi:10.5194/acp-3-361-2003, 2003. 26437
Birmili, W., Ries, L., Sohmer, R., Anastou, A., Sonntag, A., König, K., and Levin, I.: Fine and ultrafine aerosol particles at the GAW station Schneefernerhaus/Zugspitze, Gefahrst. Reinhalt. L., 69, 31–35, 2009a. 26438
Birmili, W., Weinhold, K., Nordmann, S., Wiedensohler, A., Spindler, G., Müller, K., Herrmann, H., Gnauk, T., Pitz, M., Cyrys, J., Flentje, H., Nickel, C., Kuhlbusch, T., Löschau, G., Haase, D., Meinhardt, F., Schwerin, A., Ries, L., and Wirtz, K.: Atmospheric aerosol measurements in the German Ultrafine Aerosol Network (GUAN) – Part 1: Soot and particle number size distributions, Gefahrst. Reinhalt. L., 69, 137–145, 2009b. 26437, 26438
Bodhaine, B.: Aerosol measurements at four background sites (Barrow Alaska, Mauna Loa, Hawaii, American Samoa, South Pole), J. Geophys. Res., 88, 10735–10768, 1983. 26437
Bodhaine, B.: Barrow surface aerosol: 1976–1986, Atmos. Environ., 23, 2357–2369, 1989. 26437
Bodhaine, B. and DeLuisi, J.: An aerosol climatology of Samoa, J. Atmos. Chem., 3, 107–122, doi:10.1007/BF00049371, 1985. 26437
Bodhaine, B., Deluisi, J., and Harris, J.: Aerosol measurements at the South Pole, Tellus B, 38, 223–235, 1986. 26437
Bonasoni, P., Stohl, A., Cristofanelli, P., Calzolari, F., Colombo, T., and Evangelisti, F.: Background ozone variations at Mt. Cimone Station, Atmos. Environ., 34, 5183–5189, 2000. 26437
Bonasoni, P., Laj, P., Marinoni, A., Sprenger, M., Angelini, F., Arduini, J., Bonafè, U., Calzolari, F., Colombo, T., Decesari, S., Di Biagio, C., di Sarra, A. G., Evangelisti, F., Duchi, R., Facchini, MC., Fuzzi, S., Gobbi, G. P., Maione, M., Panday, A., Roccato, F., Sellegri, K., Venzac, H., Verza, GP., Villani, P., Vuillermoz, E., and Cristofanelli, P.: Atmospheric Brown Clouds in the Himalayas: first two years of continuous observations at the Nepal Climate Observatory-Pyramid (5079 m), Atmos. Chem. Phys., 10, 7515–7531, doi:10.5194/acp-10-7515-2010, 2010. 26437
Bond, T. C., Doherty, S. J., Fahey, D. W., Forster, P. M., Berntsen, T., DeAngelo, B. J., Flanner, M. G., Ghan, S., Kärcher, B., Koch, D., Kinne, S., Kondo, Y., Quinn, P. K., Sarofim, M. C., Schultz, M. G., Schulz, M., Venkataraman, C., Zhang, H., Zhang, S., Bellouin, N., Guttikunda, S. K., Hopke, P. K., Jacobson, M. Z., Kaiser, J. W., Klimont, Z., Lohmann, U., Schwarz, J. P., Shindell, D., Storelvmo, T., Warren, S. G., and Zender, C. S.: Bounding the

ACPD
13, 26389–26450, 2013

role of black carbon in the climate system: a scientific assessment, J. Geophys. Res. D: Atmos., 118, 5380–5552, doi:10.1002/jgrd.50171, 2013. 26390

Boy, M., Kazil, J., Lovejoy, E., Guenther, A., and Kulmala, M.: Relevance of ion-induced nucleation of sulfuric acid and water in the lower troposphere over the boreal forest at northern latitudes, Atmos. Res., 90, 151–158, doi:10.1016/j.atmosres.2008.01.002, 2008. 26398

Brunke, E.-G., Ebinghaus, R., Kock, H. H., Labuschagne, C., and Slemr, F.: Emissions of mercury in southern Africa derived from long-term observations at Cape Point, South Africa, Atmos. Chem. Phys., 12, 7465–7474, doi:10.5194/acp-12-7465-2012, 2012. 26437

Cervenkova, J. and Vana, M.: Trend assessment of deposition, throughfall and runoff water chemistry at the ICP-IM station Kosetice, Czech Republic, in: Status and Perspectives of Hydrology in Small Basins, edited by: Hermann, A. and Schumann, S., 336, 103–109, IAHS Publications, 2010. 26437

Charron, A., Birmili, W., and Harrison, R.: Factors influencing new particle formation at the rural site, Harwell, UK, J. Geophys. Res.-Atmos., 112, D14210, doi:10.1029/2007JD008425, 2007. 26437

Clarke, A. and Kapustin, V.: Hemispheric aerosol vertical profiles: anthropogenic impacts on optical depth and cloud nuclei, Science, 329, 1488–1492, doi:10.1126/science.1188838, 2010. 26402, 26403, 26412, 26413, 26442, 26449

Dal Maso, M., Sogacheva, L., Anisimov, M., Arshinov, M., Baklanov, A., Belan, B., Khodzher, T., Obolkin, V., Staroverova, A., Vlasov, A., Zagaynov, V., Lushnikov, A., Lyubovtseva, Y., Riipinen, I., Kerminen, V.-M., and Kulmala, M.: Aerosol particle formation events at two Siberian stations inside the boreal forest, Boreal Environ. Res., 13, 81–92, 2008. 26437, 26438

Delene, D. and Ogren, J.: Variability of aerosol optical properties at four North American surface monitoring sites, J. Atmos. Sci., 59, 1135–1150, 2002. 26437

Dentener, F., Kinne, S., Bond, T., Boucher, O., Cofala, J., Generoso, S., Ginoux, P., Gong, S., Hoelzemann, J. J., Ito, A., Marelli, L., Penner, J. E., Putaud, J.-P., Textor, C., Schulz, M., van der Werf, G. R., and Wilson, J.: Emissions of primary aerosol and precursor gases in the years 2000 and 1750 prescribed data-sets for AeroCom, Atmos. Chem. Phys., 6, 4321–4344, doi:10.5194/acp-6-4321-2006, 2006. 26394

Engler, C., Rose, D., Wehner, B., Wiedensohler, A., Brüggemann, E., Gnauk, T., Spindler, G., Tuch, T., and Birmili, W.: Size distributions of non-volatile particle residuals (D_p < 800 nm) at a rural site in Germany and relation to air mass origin, Atmos. Chem. Phys., 7, 5785–5802, doi:10.5194/acp-7-5785-2007, 2007. 26437

ACPD
13, 26389–26450, 2013

Forster, P., Ramaswamy, V., Artaxo, P., Berntsen, T., Betts, R., Fahey, D. W., Haywood, J., Lean, J., Lowe, D. C., Myhre, G., Nganga, J., Prinn, R., Raga, G., Schulz, M., and Van Dorland, R.: Climate Change 2007, The Physical Science Basis, Contribution of Working Group I to the Fourth Assessment Report of the Intergovernmental Panel on Climate Change, Cambridge Univ. Press, Cambridge, UK, and New York, NY, USA, 2007. 26391

Fountoukis, C., Riipinen, I., Denier van der Gon, H. A. C., Charalampidis, P. E., Pilinis, C., Wiedensohler, A., O'Dowd, C., Putaud, J. P., Moerman, M., and Pandis, S. N.: Simulating ultrafine particle formation in Europe using a regional CTM: contribution of primary emissions versus secondary formation to aerosol number concentrations, Atmos. Chem. Phys., 12, 8663–8677, doi:10.5194/acp-12-8663-2012, 2012. 26391

Gaydos, T. M., Stanier, C. O., and Pandis, S. N.: Modeling of in situ ultrafine atmospheric particle formation in the eastern United States, J. Geophys. Res.-Atmos., 110, D07S12, doi:10.1029/2004JD004683, 2005. 26395

Gent, P., Danabasoglu, G., Donner, L., Holland, M., Hunke, E., Jayne, S., Lawrence, D., Neale, R., Rasch, P., Vertenstein, M., Worley, P., Yang, Z., and Zhang, M.: The community climate system model version 4, J. Climate, 24, 4973–4991, doi:10.1175/2011JCLI4083.1, 2011. 26392

Ghan, S., Easter, R., Chapman, E., Abdul-Razzak, H., Zhang, Y., Leung, L., Laulainen, N., Saylor, R., and Zaveri, R.: A physically based estimate of radiative forcing by anthropogenic sulfate aerosol, J. Geophys. Res.-Atmos., 106, 5279–5293, 2001. 26391

Gioda, A., Reyes-Rodríguez, G., Santos-Figueroa, G., Collett Jr., J., Decesari, S., Ramos, M., Bezerra Netto, H., De Aquino Neto, F., and Mayol-Bracero, O.: Speciation of water-soluble inorganic, organic, and total nitrogen in a background marine environment: cloud water, rainwater, and aerosol particles, J. Geophys. Res.-Atmos., 116, D05203, doi:10.1029/2010JD015010, 2011. 26437

Gonzàlez, Y., Rodrìguez, S., Guerra Garcìa, J., Trujillo, J., and Garcìa, R.: Ultrafine particles pollution in urban coastal air due to ship emissions, Atmos. Environ., 45, 4907–4914, doi:10.1016/j.atmosenv.2011.06.002, 2011. 26409

Gras, J. L.: CN, CCN and particle size in Southern Ocean air at Cape Grim, Atmos. Res., 35, 233–251, 1995. 26437

Gruening, C., Adam, M., Cavalli, F., Cavalli, P., Dell'Acqua, A., Martins Dos Santos, S., Pagliari, V., Roux, D., and Putaud, J.-P.: JRC Ispra EMEP – GAW Regional Station for Atmos. Res. 2008 Report, Tech. Rep. JRC55382, European Commission, available at:

ACPD
13, 26389–26450, 2013

http://publications.jrc.ec.europa.eu/repository/handle/111111111/538 (last access: September 2013), 2009. 26437
Guenther, A., Karl, T., Harley, P., Wiedinmyer, C., Palmer, P. I., and Geron, C.: Estimates of global terrestrial isoprene emissions using MEGAN (Model of Emissions of Gases and Aerosols from Nature), Atmos. Chem. Phys., 6, 3181–3210, doi:10.5194/acp-6-3181-2006, 2006. 26397
Hallar, A., Lowenthal, D., Chirokova, G., Borys, R., and Wiedinmyer, C.: Persistent daily new particle formation at a mountain-top location, Atmos. Environ., 45, 4111–4115, doi:10.1016/j.atmosenv.2011.04.044, 2011. 26437
Hallar, A., Lowenthal, D., Clegg, S., Samburova, V., Taylor, N., Mazzoleni, L., Zielinska, B., Kristensen, T., Chirokova, G., McCubbin, I., Dodson, C., and Collins, D.: Chemical and Hygroscopic Properties of Aerosol Organics at Storm Peak Laboratory, J. Geophys. Res.-Atmos., 118, 4767–4779, doi:10.1002/jgrd.50373, 2013. 26437
Hamed, A., Joutsensaari, J., Mikkonen, S., Sogacheva, L., Dal Maso, M., Kulmala, M., Cavalli, F., Fuzzi, S., Facchini, M. C., Decesari, S., Mircea, M., Lehtinen, K. E. J., and Laaksonen, A.: Nucleation and growth of new particles in Po Valley, Italy, Atmos. Chem. Phys., 7, 355–376, doi:10.5194/acp-7-355-2007, 2007. 26437
Hansen, G., Aspmo, K., Berg, T., Edvardsen, K., Fiebig, M., Kallenborn, R., Krognes, T., Lunder, C., Stebel, K., Schmidbauer, N., Solberg, S., and Yttri, K.: Atmospheric monitoring at the Norwegian Antarctic station Troll: measurement programme and first results, Polar Res., 28, 353–363, doi:10.1111/j.1751-8369.2009.00134.x, 2009. 26438
Hari, P. and Kulmala, M.: Station for Measuring Ecosystem–Atmosphere Relations (SMEAR II), Boreal Environ. Res., 10, 315–322, 2005. 26437
Heintzenberg, J., Covert, D. C., and van Dingenen, R.: Size distribution and chemical composition of marine aerosols: a compilation and review, Tellus B, 52, 1104–1122, 2000. 26403, 26415, 26450
Henne, S., Brunner, D., Folini, D., Solberg, S., Klausen, J., and Buchmann, B.: Assessment of parameters describing representativeness of air quality in-situ measurement sites, Atmos. Chem. Phys., 10, 3561–3581, doi:10.5194/acp-10-3561-2010, 2010. 26405
Hoyle, C. R., Berntsen, T., Myhre, G., and Isaksen, I. S. A.: Secondary organic aerosol in the global aerosol – chemical transport model Oslo CTM2, Atmos. Chem. Phys., 7, 5675–5694, doi:10.5194/acp-7-5675-2007, 2007. 26397

ACPD
13, 26389–26450, 2013

Iversen, T., Bentsen, M., Bethke, I., Debernard, J. B., Kirkevåg, A., Seland, Ø., Drange, H., Kristjansson, J. E., Medhaug, I., Sand, M., and Seierstad, I. A.: The Norwegian Earth System Model, NorESM1-M – Part 2: Climate response and scenario projections, Geosci. Model Dev., 6, 389–415, doi:10.5194/gmd-6-389-2013, 2013. 26393

Järvinen, E., Virkkula, A., Nieminen, T., Aalto, P. P., Asmi, E., Lanconelli, C., Busetto, M., Lupi, A., Schioppo, R., Vitale, V., Mazzola, M., Petäjä, T., Kerminen, V.-M., and Kulmala, M.: Seasonal cycle and modal structure of particle number size distribution at Dome C, Antarctica, Atmos. Chem. Phys., 13, 7473–7487, doi:10.5194/acp-13-7473-2013, 2013. 26437

Kelly, G., Taubman, B., Perry, L., Sherman, J., Soulé, P., and Sheridan, P.: Relationships between aerosols and precipitation in the southern Appalachian Mountains, Int. J. Climatol., doi:10.1002/joc.3632, 2012. 26437

Kerminen, V. M. and Kulmala, M.: Analytical formulae connecting the "real" and the "apparent" nucleation rate and the nuclei number concentration for atmospheric nucleation events, J. Aerosol Sci., 33, 609–622, 2002. 26396

Keskinen, H., Virtanen, A., Joutsensaari, J., Tsagkogeorgas, G., Duplissy, J., Schobesberger, S., Gysel, M., Riccobono, F., Slowik, J. G., Bianchi, F., Yli-Juuti, T., Lehtipalo, K., Rondo, L., Breitenlechner, M., Kupc, A., Almeida, J., Amorim, A., Dunne, E. M., Downard, A. J., Ehrhart, S., Franchin, A., Kajos, M.K., Kirkby, J., Kürten, A., Nieminen, T., Makhmutov, V., Mathot, S., Miettinen, P., Onnela, A., Petäjä, T., Praplan, A., Santos, F. D., Schallhart, S., Sipilä, M., Stozhkov, Y., Tomé, A., Vaattovaara, P., Wimmer, D., Prevot, A., Dommen, J., Donahue, N. M., Flagan, R.C., Weingartner, E., Viisanen, Y., Riipinen, I., Hansel, A., Curtius, J., Kulmala, M., Worsnop, D. R., Baltensperger, U., Wex, H., Stratmann, F., and Laaksonen, A.: Evolution of particle composition in CLOUD nucleation experiments, Atmos. Chem. Phys., 13, 5587–5600, doi:10.5194/acp-13-5587-2013, 2013. 26397

Kirkevåg, A., Iversen, T., Seland, Ø., Hoose, C., Kristjánsson, J. E., Struthers, H., Ekman, A. M. L., Ghan, S., Griesfeller, J., Nilsson, E. D., and Schulz, M.: Aerosol–climate interactions in the Norwegian Earth System Model – NorESM1-M, Geosci. Model Dev., 6, 207–244, doi:10.5194/gmd-6-207-2013, 2013. 26392, 26393, 26394, 26395, 26397, 26398, 26406, 26434

Kiss, G., Varga, B., Galambos, I., and Ganszky, I.: Characterization of water-soluble organic matter isolated from atmospheric fine aerosol, J. Geophys. Res.-Atmos., 107, 8339, doi:10.1029/2001JD000603, 2002. 26437

ACPD
13, 26389–26450, 2013

Komppula, M., Lihavainen, H., Hatakka, J., Paatero, J., Aalto, P., Kulmala, M., and Viisanen, Y.: Observations of new particle formation and size distributions at two different heights and surroundings in subarctic area in northern Finland, J. Geophys. Res., 108, 4295, doi:10.1029/2002JD002939, 2003. 26437

Komppula, M., Lihavainen, H., Hyvärinen, A.-P., Kerminen, V.-M., Panwar, T., Sharma, V., and Viisanen, Y.: Physical properties of aerosol particles at a Himalayan background site in India, J. Geophys. Res.-Atmos., 114, D12202, doi:10.1029/2008JD011007, 2009. 26437

Kristensson, A., Dal Maso, M., Swietlicki, E., Hussein, T., Zhou, J., Kerminen, V.-M., and Kulmala, M.: Characterization of new particle formation events at a background site in southern Sweden: relation to air mass history, Tellus B, 60, 330–344, doi:10.1111/j.1600-0889.2008.00345.x, 2008. 26438

Kulmala, M., Lehtinen, K. E. J., and Laaksonen, A.: Cluster activation theory as an explanation of the linear dependence between formation rate of 3nm particles and sulphuric acid concentration, Atmos. Chem. Phys., 6, 787–793, doi:10.5194/acp-6-787-2006, 2006. 26395

Kulmala, M., Asmi, A., Lappalainen, H. K., Baltensperger, U., Brenguier, J.-L., Facchini, M. C., Hansson, H.-C., Hov, Ø., O'Dowd, C. D., Pöschl, U., Wiedensohler, A., Boers, R., Boucher, O., de Leeuw, G., Denier van der Gon, H. A. C., Feichter, J., Krejci, R., Laj, P., Lihavainen, H., Lohmann, U., McFiggans, G., Mentel, T., Pilinis, C., Riipinen, I., Schulz, M., Stohl, A., Swietlicki, E., Vignati, E., Alves, C., Amann, M., Ammann, M., Arabas, S., Artaxo, P., Baars, H., Beddows, D. C. S., Bergström, R., Beukes, J. P., Bilde, M., Burkhart, J. F., Canonaco, F., Clegg, S. L., Coe, H., Crumeyrolle, S., D'Anna, B., Decesari, S., Gilardoni, S., Fischer, M., Fjaeraa, A. M., Fountoukis, C., George, C., Gomes, L., Halloran, P., Hamburger, T., Harrison, R. M., Herrmann, H., Hoffmann, T., Hoose, C., Hu, M., Hyvärinen, A., Hõrrak, U., Iinuma, Y., Iversen, T., Josipovic, M., Kanakidou, M., Kiendler-Scharr, A., Kirkevåg, A., Kiss, G., Klimont, Z., Kolmonen, P., Komppula, M., Kristjánsson, J.-E., Laakso, L., Laaksonen, A., Labonnote, L., Lanz, V. A., Lehtinen, K. E. J., Rizzo, L. V., Makkonen, R., Manninen, H. E., McMeeking, G., Merikanto, J., Minikin, A., Mirme, S., Morgan, W. T., Nemitz, E., O'Donnell, D., Panwar, T. S., Pawlowska, H., Petzold, A., Pienaar, J. J., Pio, C., Plass-Duelmer, C., Prévôt, A. S. H., Pryor, S., Reddington, C. L., Roberts, G., Rosenfeld, D., Schwarz, J., Seland, Ø., Sellegri, K., Shen, X. J., Shiraiwa, M., Siebert, H., Sierau, B., Simpson, D., Sun, J. Y., Topping, D., Tunved, P., Vaattovaara, P., Vakkari, V., Veefkind, J. P., Visschedijk, A., Vuollekoski, H., Vuolo, R., Wehner, B., Wildt, J., Woodward, S., Worsnop, D. R., van Zadelhoff, G.-J., Zardini, A. A., Zhang, K., van Zyl, P. G., Kerminen, V.-M., S Carslaw, K.,

ACPD
13, 26389–26450, 2013

and Pandis, S. N.: General overview: European Integrated project on Aerosol Cloud Climate and Air Quality interactions (EUCAARI) – integrating aerosol research from nano to global scales, Atmos. Chem. Phys., 11, 13061–13143, doi:10.5194/acp-11-13061-2011, 2011. 26391

Kyrö, E.-M., Kerminen, V.-M., Virkkula, A., Dal Maso, M., Parshintsev, J., Ruíz-Jimenez, J., Forsström, L., Manninen, H. E., Riekkola, M.-L., Heinonen, P., and Kulmala, M.: Antarctic new particle formation from continental biogenic precursors, Atmos. Chem. Phys., 13, 3527–3546, doi:10.5194/acp-13-3527-2013, 2013. 26408

Laakso, L., Merikanto, J., Vakkari, V., Laakso, H., Kulmala, M., Molefe, M., Kgabi, N., Mabaso, D., Carslaw, K. S., Spracklen, D. V., Lee, L. A., Reddington, C. L., and Kerminen, V.-M.: Boundary layer nucleation as a source of new CCN in savannah environment, Atmos. Chem. Phys., 13, 1957–1972, doi:10.5194/acp-13-1957-2013, 2013. 26437

Labuschagne, C., Brunke, E.-G., Beukes, J., van Zyl, P., and Laakso, L.: Aerosols in a coastal environment: what does 6 years of measurements tell us?, in: South African Society for Atmospheric Sciences, Cape Town – 28th Annual Conference, 26–27 September 2012, ISBN 978-0-620-53375-1, 2012. 26437

Lamarque, J.-F., Bond, T. C., Eyring, V., Granier, C., Heil, A., Klimont, Z., Lee, D., Liousse, C., Mieville, A., Owen, B., Schultz, M. G., Shindell, D., Smith, S. J., Stehfest, E., Van Aardenne, J., Cooper, O. R., Kainuma, M., Mahowald, N., McConnell, J. R., Naik, V., Riahi, K., and van Vuuren, D. P.: Historical (1850–2000) gridded anthropogenic and biomass burning emissions of reactive gases and aerosols: methodology and application, Atmos. Chem. Phys., 10, 7017–7039, doi:10.5194/acp-10-7017-2010, 2010. 26394

Langley, L., Leaitch, W. R., Lohmann, U., Shantz, N. C., and Worsnop, D. R.: Contributions from DMS and ship emissions to CCN observed over the summertime North Pacific, Atmos. Chem. Phys., 10, 1287–1314, doi:10.5194/acp-10-1287-2010, 2010. 26411

Lehtinen, K., Dal Maso, M., Kulmala, M., and Kerminen, V.-M.: Estimating nucleation rates from apparent particle formation rates and vice versa: revised formulation of the Kerminen-Kulmala equation, J. Aerosol Sci., 38, 988–994, doi:10.1016/j.jaerosci.2007.06.009, 2007. 26395, 26396

Lohmann, U. and Feichter, J.: Global indirect aerosol effects: a review, Atmos. Chem. Phys., 5, 715–737, doi:10.5194/acp-5-715-2005, 2005. 26391

Lucas, D. and Akimoto, H.: Evaluating aerosol nucleation parameterizations in a global atmospheric model, Geophys. Res. Lett., 33, L10808, doi:10.1029/2006GL025672, 2006. 26395

ACPD
13, 26389–26450, 2013

Makkonen, R., Asmi, A., Korhonen, H., Kokkola, H., Järvenoja, S., Räisänen, P., Lehtinen, K. E. J., Laaksonen, A., Kerminen, V.-M., Järvinen, H., Lohmann, U., Bennartz, R., Feichter, J., and Kulmala, M.: Sensitivity of aerosol concentrations and cloud properties to nucleation and secondary organic distribution in ECHAM5-HAM global circulation model, Atmos. Chem. Phys., 9, 1747–1766, doi:10.5194/acp-9-1747-2009, 2009. 26395

Makkonen, R., Asmi, A., Kerminen, V.-M., Boy, M., Arneth, A., Guenther, A., and Kulmala, M.: BVOC-aerosol-climate interactions in the global aerosol-climate model ECHAM5.5-HAM2, Atmos. Chem. Phys., 12, 10077–10096, doi:10.5194/acp-12-10077-2012, 2012a. 26400, 26416

Makkonen, R., Asmi, A., Kerminen, V.-M., Boy, M., Arneth, A., Hari, P., and Kulmala, M.: Air pollution control and decreasing new particle formation lead to strong climate warming, Atmos. Chem. Phys., 12, 1515–1524, doi:10.5194/acp-12-1515-2012, 2012b. 26392

Mann, G. W., Carslaw, K. S., Spracklen, D. V., Ridley, D. A., Manktelow, P. T., Chipperfield, M. P., Pickering, S. J., and Johnson, C. E.: Description and evaluation of GLOMAP-mode: a modal global aerosol microphysics model for the UKCA composition-climate model, Geosci. Model Dev., 3, 519–551, doi:10.5194/gmd-3-519-2010, 2010. 26391

Marinoni, A., Cristofanelli, F., Calzolari, F., Bonafè, U., and Bonasoni, P.: Continous measurements of aerosol physical parameters at the Mt. Cimone GAW station (2165 m a.s.l., Italy), Sci. Total Environ., 391, 231–251, 2008. 26437

Merikanto, J., Spracklen, D. V., Mann, G. W., Pickering, S. J., and Carslaw, K. S.: Impact of nucleation on global CCN, Atmos. Chem. Phys., 9, 8601–8616, doi:10.5194/acp-9-8601-2009, 2009. 26392

Metzger, A., Verheggen, B., Dommen, J., Duplissy, J., Prevot, A. S. H., Weingartner, E., Riipinen, I., Kulmala, M., Spracklen, D. V., Carslaw, K. S., and Baltensperger, U.: Evidence for the role of organics in aerosol particle formation under atmospheric conditions, P. Natl. Acad. Sci. USA, 107, 6646–6651, doi:10.1073/pnas.0911330107, 2010. 26400

Mihalopoulos, N., Stephanou, E., Kanakidou, M., Pilitsidis, S., and Bousquet, P.: Tropospheric aerosol ionic composition in the Eastern Mediterranean region, Tellus B, 49, 314–326, 1997. 26437

Myhre, G., Samset, B. H., Schulz, M., Balkanski, Y., Bauer, S., Berntsen, T. K., Bian, H., Bellouin, N., Chin, M., Diehl, T., Easter, R. C., Feichter, J., Ghan, S. J., Hauglustaine, D., Iversen, T., Kinne, S., Kirkevåg, A., Lamarque, J.-F., Lin, G., Liu, X., Lund, M. T., Luo, G., Ma, X., van Noije, T., Penner, J. E., Rasch, P. J., Ruiz, A., Seland, Ø., Skeie, R. B., Stier, P.,

ACPD
13, 26389–26450, 2013

Takemura, T., Tsigaridis, K., Wang, P., Wang, Z., Xu, L., Yu, H., Yu, F., Yoon, J.-H., Zhang, K., Zhang, H., and Zhou, C.: Radiative forcing of the direct aerosol effect from AeroCom Phase II simulations, Atmos. Chem. Phys., 13, 1853–1877, doi:10.5194/acp-13-1853-2013, 2013. 26390

Nojarov, P., Ivanov, P., Kalapov, I., Penev, I., and Drenska, M.: Connection between ozone concentration and atmosphere circulation at peak Moussala, Theor. Appl. Climatol., 98, 201–208, doi:10.1007/s00704-009-0173-2, 2009. 26437

O'Dowd, C. and Hoffmann, T.: Coastal new particle formation: a review of the current state-of-the-art, Environ. Chem., 2, 245–255, doi:10.1071/EN05077, 2005. 26407

O'Dowd, C. D., Hill, M. K., Smith, M. H., Geever, M., and Jennings, S. G.: New particle formation: nucleation rates and spatial scales in the coastal environment, J. Aerosol Sci., 29, S183–S184, 1998. 26437

Oleson, K., Lawrence, D. M., Bonan, G. B., Flanner, M., Kluzek, E., Lawrence, P., Levis, S., Swenson, S., Thornton, P., Dai, A., Decker, M., Dickinson, R., Feddema, J., Heald, C., Hoffman, F., Lamarque, J., Mahowald, N., Niu, G., Qian, T., Randerson, J., Running, S., Sakaguchi, K., Slater, A., Stockli, R., Wang, A., Yang, Z., Zeng, X., and Zeng, X.: Technical Description of Version 4.0 of the Community Land Model (CLM), NCAR Technical Note, NCAR/TN-478+STR, 2010. 26393

Paasonen, P., Nieminen, T., Asmi, E., Manninen, H. E., Petäjä, T., Plass-Dülmer, C., Flentje, H., Birmili, W., Wiedensohler, A., Hõrrak, U., Metzger, A., Hamed, A., Laaksonen, A., Facchini, M. C., Kerminen, V.-M., and Kulmala, M.: On the roles of sulphuric acid and low-volatility organic vapours in the initial steps of atmospheric new particle formation, Atmos. Chem. Phys., 10, 11223–11242, doi:10.5194/acp-10-11223-2010, 2010. 26395, 26400

Pandolfi, M., Cusack, M., Alastuey, A., and Querol, X.: Variability of aerosol optical properties in the Western Mediterranean Basin, Atmos. Chem. Phys., 11, 8189–8203, doi:10.5194/acp-11-8189-2011, 2011. 26437

Pierce, J. R. and Adams, P. J.: Efficiency of cloud condensation nuclei formation from ultrafine particles, Atmos. Chem. Phys., 7, 1367–1379, doi:10.5194/acp-7-1367-2007, 2007. 26399

Pierce, J. R. and Adams, P. J.: Uncertainty in global CCN concentrations from uncertain aerosol nucleation and primary emission rates, Atmos. Chem. Phys., 9, 1339–1356, doi:10.5194/acp-9-1339-2009, 2009. 26395

Reddington, C. L., Carslaw, K. S., Spracklen, D. V., Frontoso, M. G., Collins, L., Merikanto, J., Minikin, A., Hamburger, T., Coe, H., Kulmala, M., Aalto, P., Flentje, H., Plass-Dülmer, C., Bir-

ACPD
13, 26389–26450, 2013

mili, W., Wiedensohler, A., Wehner, B., Tuch, T., Sonntag, A., O'Dowd, C. D., Jennings, S. G., Dupuy, R., Baltensperger, U., Weingartner, E., Hansson, H.-C., Tunved, P., Laj, P., Sellegri, K., Boulon, J., Putaud, J.-P., Gruening, C., Swietlicki, E., Roldin, P., Henzing, J. S., Moerman, M., Mihalopoulos, N., Kouvarakis, G., Ždímal, V., Zíková, N., Marinoni, A., Bonasoni, P., and Duchi, R.: Primary versus secondary contributions to particle number concentrations in the European boundary layer, Atmos. Chem. Phys., 11, 12007–12036, doi:10.5194/acp-11-12007-2011, 2011. 26398

Reddington, C. L., McMeeking, G., Mann, G. W., Coe, H., Frontoso, M. G., Liu, D., Flynn, M., Spracklen, D. V., and Carslaw, K. S.: The mass and number size distributions of black carbon aerosol over Europe, Atmos. Chem. Phys., 13, 4917–4939, doi:10.5194/acp-13-4917-2013, 2013. 26398, 26399

Riipinen, I., Pierce, J. R., Yli-Juuti, T., Nieminen, T., Häkkinen, S., Ehn, M., Junninen, H., Lehtipalo, K., Petäjä, T., Slowik, J., Chang, R., Shantz, N. C., Abbatt, J., Leaitch, W. R., Kerminen, V.-M., Worsnop, D. R., Pandis, S. N., Donahue, N. M., and Kulmala, M.: Organic condensation: a vital link connecting aerosol formation to cloud condensation nuclei (CCN) concentrations, Atmos. Chem. Phys., 11, 3865–3878, doi:10.5194/acp-11-3865-2011, 2011. 26397

Rissler, J., Vestin, A., Swietlicki, E., Fisch, G., Zhou, J., Artaxo, P., and Andreae, M. O.: Size distribution and hygroscopic properties of aerosol particles from dry-season biomass burning in Amazonia, Atmos. Chem. Phys., 6, 471–491, doi:10.5194/acp-6-471-2006, 2006. 26412

Rodríguez, S., González, Y., Cuevas, E., Ramos, R., Romero, P. M., Abreu-Afonso, J., and Redondas, A.: Atmospheric nanoparticle observations in the low free troposphere during upward orographic flows at Izaña Mountain Observatory, Atmos. Chem. Phys., 9, 6319–6335, doi:10.5194/acp-9-6319-2009, 2009. 26437

Russchenberg, H., Bosveld, F., Swart, D., Ten Brink, H., De Leeuw, G., Uijlenhoet, R., Arbesser-Rastburg, B., Van Der Marel, H., Ligthart, L., Boers, R., and Apituley, A.: Ground-based atmospheric remote sensing in the Netherlands: European outlook, IEICE T. Commun., E88-B, 2252–2257, doi:10.1093/ietcom/e88-b.6.2252, 2005. 26437

Schmeissner, T., Krejci, R., Ström, J., Birmili, W., Wiedensohler, A., Hochschild, G., Gross, J., Hoffmann, P., and Calderon, S.: Analysis of number size distributions of tropical free tropospheric aerosol particles observed at Pico Espejo (4765 m a.s.l.), Venezuela, Atmos. Chem. Phys., 11, 3319–3332, doi:10.5194/acp-11-3319-2011, 2011. 26437

ACPD
13, 26389–26450, 2013

Shaw, S., Gantt, B., and Meskhidze, N.: Production and emissions of marine isoprene and monoterpenes: a review, Advances in Meteorology, 2010, 408696, doi:10.1155/2010/408696, 2010. 26394

Sihto, S.-L., Kulmala, M., Kerminen, V.-M., Dal Maso, M., Petäjä, T., Riipinen, I., Korhonen, H., Arnold, F., Janson, R., Boy, M., Laaksonen, A., and Lehtinen, K. E. J.: Atmospheric sulphuric acid and aerosol formation: implications from atmospheric measurements for nucleation and early growth mechanisms, Atmos. Chem. Phys., 6, 4079–4091, doi:10.5194/acp-6-4079-2006, 2006. 26395

Spracklen, D. V., Pringle, K. J., Carslaw, K. S., Chipperfield, M. P., and Mann, G. W.: A global off-line model of size-resolved aerosol microphysics: I. Model development and prediction of aerosol properties, Atmos. Chem. Phys., 5, 2227–2252, doi:10.5194/acp-5-2227-2005, 2005. 26391

Spracklen, D. V., Carslaw, K. S., Kulmala, M., Kerminen, V.-M., Mann, G. W., and Sihto, S.-L.: The contribution of boundary layer nucleation events to total particle concentrations on regional and global scales, Atmos. Chem. Phys., 6, 5631–5648, doi:10.5194/acp-6-5631-2006, 2006. 26395

Spracklen, D. V., Carslaw, K. S., Merikanto, J., Mann, G. W., Reddington, C. L., Pickering, S., Ogren, J. A., Andrews, E., Baltensperger, U., Weingartner, E., Boy, M., Kulmala, M., Laakso, L., Lihavainen, H., Kivekäs, N., Komppula, M., Mihalopoulos, N., Kouvarakis, G., Jennings, S. G., O'Dowd, C., Birmili, W., Wiedensohler, A., Weller, R., Gras, J., Laj, P., Sellegri, K., Bonn, B., Krejci, R., Laaksonen, A., Hamed, A., Minikin, A., Harrison, R. M., Talbot, R., and Sun, J.: Explaining global surface aerosol number concentrations in terms of primary emissions and particle formation, Atmos. Chem. Phys., 10, 4775–4793, doi:10.5194/acp-10-4775-2010, 2010. 26405, 26416, 26437

Spracklen, D. V., Jimenez, J. L., Carslaw, K. S., Worsnop, D. R., Evans, M. J., Mann, G. W., Zhang, Q., Canagaratna, M. R., Allan, J., Coe, H., McFiggans, G., Rap, A., and Forster, P.: Aerosol mass spectrometer constraint on the global secondary organic aerosol budget, Atmos. Chem. Phys., 11, 12109–12136, doi:10.5194/acp-11-12109-2011, 2011. 26394

Stier, P., Feichter, J., Kinne, S., Kloster, S., Vignati, E., Wilson, J., Ganzeveld, L., Tegen, I., Werner, M., Balkanski, Y., Schulz, M., Boucher, O., Minikin, A., and Petzold, A.: The aerosol-climate model ECHAM5-HAM, Atmos. Chem. Phys., 5, 1125–1156, doi:10.5194/acp-5-1125-2005, 2005. 26391, 26399

ACPD
13, 26389–26450, 2013

Ström, J., Umegård, J., Tørseth, K., Tunved, P., Hansson, H.-C., Holmén, K., Wismann, V., Herber, A., and König-Langlo, G.: One year of particle size distribution and aerosol chemical composition measurements at the Zeppelin Station, Svalbard, March 2000–March 2001, Phys. Chem. Earth, 28, 1181–1190, doi:10.1016/j.pce.2003.08.058, 2003. 26438

Struthers, H., Ekman, A. M. L., Glantz, P., Iversen, T., Kirkevåg, A., Mårtensson, E. M., Seland, Ø., and Nilsson, E. D.: The effect of sea ice loss on sea salt aerosol concentrations and the radiative balance in the Arctic, Atmos. Chem. Phys., 11, 3459–3477, doi:10.5194/acp-11-3459-2011, 2011. 26394

Tunved, P., Ström, J., and Hansson, H.-C.: An investigation of processes controlling the evolution of the boundary layer aerosol size distribution properties at the Swedish background station Aspvreten, Atmos. Chem. Phys., 4, 2581–2592, doi:10.5194/acp-4-2581-2004, 2004. 26437

Tunved, P., Ström, J., and Krejci, R.: Arctic aerosol life cycle: linking aerosol size distributions observed between 2000 and 2010 with air mass transport and precipitation at Zeppelin station, Ny-Ålesund, Svalbard, Atmos. Chem. Phys., 13, 3643–3660, doi:10.5194/acp-13-3643-2013, 2013. 26438

Ulevicius, V., Byčenkienė, S., Remeikis, V., Garbaras, A., Kecorius, S., Andriejauskienė, J., Jasinevičienė, D., and Mocnik, G.: Characterization of pollution events in the East Baltic region affected by regional biomass fire emissions, Atmos. Res., 98, 190–200, doi:10.1016/j.atmosres.2010.03.021, 2010. 26437

Vehkamäki, H., Kulmala, M., Napari, I., Lehtinen, K. E. J., Timmreck, C., Noppel, M., and Laaksonen, A.: An improved parameterization for sulfuric acid/water nucleation rates for tropospheric and stratospheric conditions, J. Geophys. Res., 107, 4622–4631, 2002. 26395

Veltkamp, P., Hansen, K., Barkley, R., and Sievers, R.: Principal component analysis of summertime organic aerosols at Niwot Ridge, Colorado, J. Geophys. Res.-Atmos., 101, 19495–19504, 1996. 26437

Venzac, H., Sellegri, K., Laj, P., Villani, P., Bonasoni, P., Marinoni, A., Cristofanelli, P., Calzolari, F., Fuzzi, S., Decesari, S., Facchini, M.-C., Vuillermoz, E., and Verza, G.: High frequency new particle formation in the Himalayas, P. Natl. Acad. Sci. USA, 105, 15666–15671, doi:10.1073/pnas.0801355105, 2008. 26437

Venzac, H., Sellegri, K., Villani, P., Picard, D., and Laj, P.: Seasonal variation of aerosol size distributions in the free troposphere and residual layer at the puy de Dôme station, France, Atmos. Chem. Phys., 9, 1465–1478, doi:10.5194/acp-9-1465-2009, 2009. 26437

ACPD
13, 26389–26450, 2013

Vertenstein, M., Craig, T., Middleton, A., Feddema, D., and Fischer, C.: CCSM4.0 User's Guide, available at: http://www.cesm.ucar.edu/models/ccsm4.0/ccsm_doc/book1.html (last access: September 2013), 2010. 26392

Von Salzen, K., Leighton, H., Ariya, P., Barrie, L., Gong, S., Blanchet, J.-P., Spacek, L., Lohmann, U., and Kleinman, L.: Sensitivity of sulphate aerosol size distributions and CCN concentrations over North America to SO_x emissions and H_2O_2 concentrations, J. Geophys. Res.-Atmos., 105, 9741–9765, 2000. 26391

Wai, K., Lin, N.-H., Wang, S.-H., and Dokiya, Y.: Rainwater chemistry at a high-altitude station, Mt. Lulin, Taiwan: comparison with a background station, Mt. Fuji, J. Geophys. Res.-Atmos., 113, D23S34, doi:10.1029/2006JD008248, 2008. 26437

Weingartner, E., Nyecki, S., and Baltensberger, U.: Seasonal and diurnal variation of aerosol size distributions ($10 < D < 750$ nm) at a high-alpine site (Jungfraujoch 3580 m a.s.l.), J. Geophys. Res., 104, 26809–26820, 1999. 26437

Weller, R., Minikin, A., Wagenbach, D., and Dreiling, V.: Characterization of the inter-annual, seasonal, and diurnal variations of condensation particle concentrations at Neumayer, Antarctica, Atmos. Chem. Phys., 11, 13243–13257, doi:10.5194/acp-11-13243-2011, 2011. 26437

Yli-Juuti, T., Nieminen, T., Hirsikko, A., Aalto, P. P., Asmi, E., Hõrrak, U., Manninen, H. E., Patokoski, J., Dal Maso, M., Petäjä, T., Rinne, J., Kulmala, M., and Riipinen, I.: Growth rates of nucleation mode particles in Hyytiälä during 2003–2009: variation with particle size, season, data analysis method and ambient conditions, Atmos. Chem. Phys., 11, 12865–12886, doi:10.5194/acp-11-12865-2011, 2011. 26397, 26398

Yu, F., Wang, Z., Luo, G., and Turco, R.: Ion-mediated nucleation as an important global source of tropospheric aerosols, Atmos. Chem. Phys., 8, 2537–2554, doi:10.5194/acp-8-2537-2008, 2008. 26395

Zhang, K., O'Donnell, D., Kazil, J., Stier, P., Kinne, S., Lohmann, U., Ferrachat, S., Croft, B., Quaas, J., Wan, H., Rast, S., and Feichter, J.: The global aerosol-climate model ECHAM-HAM, version 2: sensitivity to improvements in process representations, Atmos. Chem. Phys., 12, 8911–8949, doi:10.5194/acp-12-8911-2012, 2012. 26399

Ziemba, L., Griffin, R., and Talbot, R.: Observations of elevated particle number concentration events at a rural site in New England, J. Geophys. Res.-Atmos., 111, D23S34, doi:10.1029/2006JD007607, 2006. 26438

ACPD
13, 26389–26450, 2013

Table 1. Simulated sensitivity experiments. The simulated climate is identical in all experiments except ActNuc_BC24_Online, where aerosol-climate interactions are switched on.

Short name	Nucleation	BSOA	BC_{FF} radii	Additional information
NorESM1-M	On*	On	11.8 nm	As in Kirkevåg et al. (2013)
NoNuc_BC12	Off	On	11.8 nm	
NoNuc_BC24	Off	On	23.6 nm	
ActNuc_BC12	Eq. (1)	On	11.8 nm	
ActNuc_BC24	Eq. (1)	On	23.6 nm	
OrgNuc_BC12	Eq. (4)	On	11.8 nm	
ActNuc_BC12_NoSOA	Eq. (1)	Off	11.8 nm	
ActNuc_BC24_NoSOA	Eq. (1)	Off	23.6 nm	
ActNuc_BC24_Online	Eq. (1)	On	23.6 nm	Aerosols affect model meteorology
ActNuc_BC24_Nuc10	Eq. (1)	On	23.6 nm	SO_4 nucleation mode diameter set to 10 nm

* Original NorESM1-M assumed that after condensation, all excess sulfuric acid nucleates as new particles.

ACPD
13, 26389–26450, 2013

Table 2. Global average surface-level number concentrations from model experiments.

	Global	Land	Ocean
NorESM1-M	1534	2230	587
NoNuc_BC12	973	1489	271
NoNuc_BC24	618	890	248
ActNuc_BC12	1444	2205	409
ActNuc_BC24	1179	1754	398
OrgNuc_BC12	1519	2340	403
ActNuc_BC12_NoSoa	1238	1858	396
ActNuc_BC24_NoSOA	960	1384	384
ActNuc_BC24_Online	1163	1738	381
ActNuc_BC24_Nuc10	2155	3254	660

ACPD
13, 26389–26450, 2013

Table 3. Mean bias (%) and correlation coefficient R^2 calculated over all stations and six regions.

	All		Arctic		Marine		Antarctic		High altitude		Remote		Rural	
	BIAS(%)	R^2	BIAS(%)	R^2	BIAS(%)	R^2	BIAS(%)	R^2	BIAS(%)	R^2	BIAS(%)	R^2	BIAS(%)	R^2
NorESM1-M	33	0.38	39	0.43	47	0.17	16	0.88	88	0.49	−8	0.36	20	0.27
NoNuc_BC12	−27	0.30	−24	0.25	−31	0.09	−47	0.82	−45	0.40	−34	0.32	−6	0.18
NoNuc_BC24	−64	0.35	−37	0.31	−53	0.15	−47	0.81	−69	0.39	−66	0.35	−69	0.31
ActNuc_BC12	20	0.40	38	0.48	39	0.13	−39	0.83	22	0.50	11	0.38	27	0.34
ActNuc_BC24	−5	0.41	31	0.51	25	0.12	−39	0.83	9	0.51	−11	0.38	−18	0.38
OrgNuc_BC12	20	0.39	54	0.43	41	0.13	−39	0.83	20	0.49	12	0.36	25	0.34
ActNuc_BC12_NoSOA	2	0.38	−15	0.30	11	0.15	−40	0.83	10	0.47	−17	0.48	17	0.29
ActNuc_BC24_NoSOA	−25	0.42	−24	0.41	−5	0.15	−41	0.83	−3	0.48	−41	0.53	−31	0.38
ActNuc_BC24_Online	−8	0.43	22	0.62	23	0.15	−36	0.76	4	0.51	−11	0.40	−20	0.39
ActNuc_BC24_Nuc10	81	0.38	349	0.47	160	0.10	17	0.53	94	0.45	48	0.38	31	0.37

ACPD
13, 26389–26450, 2013

Table 4. Description of surface sites used in the model evaluation. Source of data: EBAS (E), WDCA (W), NOAA (N), Spracklen et al. (2010) (S), published data (P). The minimum cut-off diameter dp_{cut} as well as covered measurement years are indicated for each station.

Station	Lon	Lat	m a.s.l.	Years	dp_{cut} (nm)	Source	Reference
Aspvreten	17.4° E	58.8° N	25	2000–2006	10	S	Tunved et al. (2004)
Point Barrow	156.6° W	71.3° N	11	1997–2011	14	E	Bodhaine (1989)
Birkenes	8.2° E	58.4° N	190	2006, 2008–2011	10	E	Amundsen et al. (1992)
Bondville	88.4° W	40.0° N	213	1997–2003	14	E	Delene and Ogren (2002)
Boone	81.7° W	36.2° N	1100	2009–2011	10	E	Kelly et al. (2012)
Bösel	7.9° E	53.0° N	17	2010–2011	10	E	Birmili et al. (2009b)
Botsalano	25.8° E	25.5° S	1424	2006–2007	12	P	Laakso et al. (2013)
Cabauw	4.9° E	52.0° N	60	2009–2010	10	E	Russchenberg et al. (2005)
Cape Grim	144.7° E	40.6° S	94	2002–2005	3	W	Gras (1995)
Cape Point	18.5° E	34.4° S	230	2006–2011	10	E	Brunke et al. (2012); Labuschagne et al. (2012)
Cape San Juan	65.6° W	18.4° N	66	2005–2011	10	E	Gioda et al. (2011)
Cape St. James	131.0° W	51.9° N	92	2005	10	N	
Castle Springs	71.3° W	43.7° N	406	2001–2008	7	S	
Dome C	123.4° E	75.1° S	3200	2007–2009	10	P	Järvinen et al. (2013)
Finokalia	25.7° E	35.3° N	250	2009–2010	10	E	Mihalopoulos et al. (1997)
Harwell	1.3° W	51.6° N	126	2006–2007, 2010	10	E	Charron et al. (2007)
Hohenpeissenberg	11.0° E	47.8° N	980	1998–2000	10	E	Birmili et al. (2003)
Hyytiälä	24.3° E	61.9° N	180	1997–2000	10	E	Hari and Kulmala (2005)
Ispra	8.6° E	45.8° N	0	2008–2010	10	E	Gruening et al. (2009)
Izana	16.5° W	28.3° N	2373	2006–2010	10	E	Rodríguez et al. (2009)
Jungfraujoch	8.0° E	46.5° N	3580	2008–2009	10	E	Weingartner et al. (1999)
Kosetice	15.1° E	49.6° N	534	2009–2011	10	E	Cervenkova and Vana (2010); Asmi et al. (2011)
K-Puszta	19.6° E	47.0° N	125	2006–2007	10	E	Kiss et al. (2002)
Listvyanka	104.9° E	51.9° N	750	2005–2006	3	S	Dal Maso et al. (2008)
Lulin	120.9° E	23.5° N	2862	2008–2012	10	E	Wai et al. (2008)
Mace Head	9.9° W	53.3° N	5	2002–2010	10	E	O'Dowd et al. (1998)
Marikana	27.5° E	25.7° S	1170	2008–2010	12	P	Laakso et al. (2013)
Mauna Loa	155.6° W	19.5° N	3397	1999–2003	14	E	Bodhaine (1983)
Melpitz	12.9° E	51.5° N	84	1996–1997, 2003	3	S	Engler et al. (2007)
Montseny	2.4° E	41.8° N	720	2009	10	E	Pandolfi et al. (2011)
Mount Cimone	10.7° E	44.2° N	2165	2010–2011	10	E	Bonasoni et al. (2000); Marinoni et al. (2008)
Mount Washington	71.3° W	44.3° N	1910	2002–2005	10	S	Venzac et al. (2008)
Moussala	23.6° E	42.2° N	2925	2009–2010	10	E	Nojarov et al. (2009)
India Himalaya	79.6° E	29.4° N	2180	2005–2008	10	S	Komppula et al. (2009)
Nepal C.O.	86.8° E	27.9° N	5079	2007–2008	10	S	Venzac et al. (2008); Bonasoni et al. (2010)
Neumayer	8.3° W	70.7° S	42	1995–2010	14	E/W	Weller et al. (2011)
Niwotridge	105.5° W	40.0° N	3000	1993–1995	10	N	Veltkamp et al. (1996)
Pallas	24.1° E	68.0° N	340	2008–2010	10	E	Komppula et al. (2003)
Pico Espejo	71.1° W	8.5° N	4775	2007–2009	10	S	Schmeissner et al. (2011)
Po Valley	11.6° E	44.7° N	11	2002–2006	3	S	Hamed et al. (2007)
Preila	21.1° E	55.4° N	5	2009–2010	10	E	Ulevicius et al. (2010)
Puy de Dome	3.0° E	45.8° N	1465	2009–2011	10	E	Venzac et al. (2009)
Sable Island	60.0° W	43.9° N	5	1996–1999	10	E	Delene and Ogren (2002)
Samoa	170.6° W	14.3° S	77	1997–1999, 2004–2006	14	E	Bodhaine and DeLuisi (1985)
Schauinsland	7.9° E	47.9° N	1205	2006–2010	10	E	Birmili et al. (2009b)
Southern Great Plains	97.5° W	36.6° N	320	1997–2003	10	E	Delene and Ogren (2002)
South Pole	24.8° W	90.0° S	2810	1997–2003	14	E	Bodhaine et al. (1986)
Storm Peak	106.7° W	40.4° N	3210	1998–2010	10	E	Hallar et al. (2011, 2013)

ACPD
13, 26389–26450, 2013

Table 4. Continued.

Station	Lon	Lat	m a.s.l.	Years	dp_{cut} (nm)	Source	Reference
Taunus Observatory	8.4° E	50.2° N	810	2008–2009	10	S	
Thompson Farm	289.1° E	43.1° N	75	2001–2009	7	S	Ziemba et al. (2006)
Tomsk	85.1° E	56.5° N	170	2005–2006	3	S	Dal Maso et al. (2008)
Trinidad Head	124.2° W	41.0° N	107	2002–2011	14	E	Allan et al. (2004)
Troll	2.5° E	72.0° S	1309	2007–2009, 2011–2012	10	E	Hansen et al. (2009)
Utö	21.4° E	59.8° N	8	2003–2006	7	S	Dal Maso et al. (2008)
Värriö	29.6° E	67.8° N	400	1998–2006	8	S	Dal Maso et al. (2008)
Vavihill	13.2° E	56.0° N	172	2010–2011	10	E	Kristensson et al. (2008)
Waldhof	10.8° E	52.8° N	75	2009–2011	10	E	Birmili et al. (2009b)
Weybourne	1.1° E	53.0° N	0	2005	10	S	
Zeppelin	11.9° E	78.9° N	474	2000–2010	20	P	Ström et al. (2003); Tunved et al. (2013)
Zugspitze	11.0° E	47.4° N	2650	2004–2007	12	E	Birmili et al. (2009a)

ACPD
13, 26389–26450, 2013

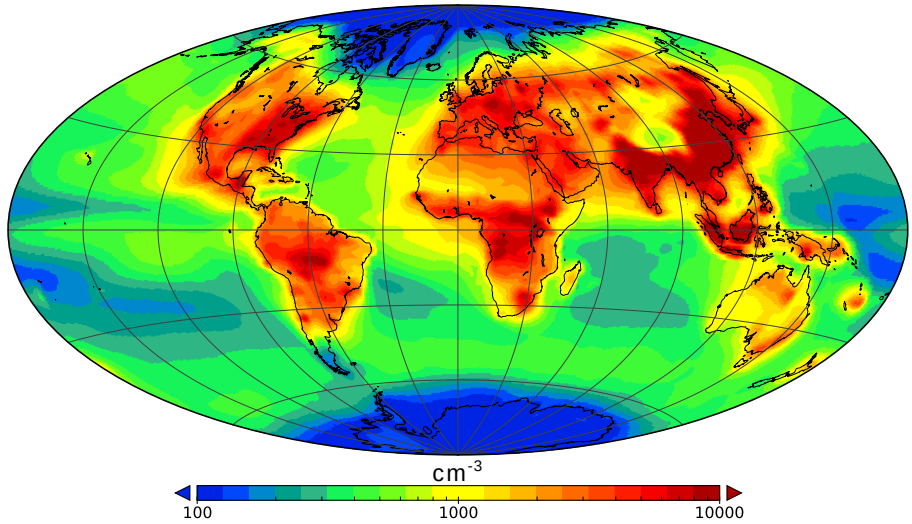

Fig. 1. Annual mean surface-level aerosol number concentration (cm^{-3}) from ActNuc_BC12 simulation.

ACPD
13, 26389–26450, 2013

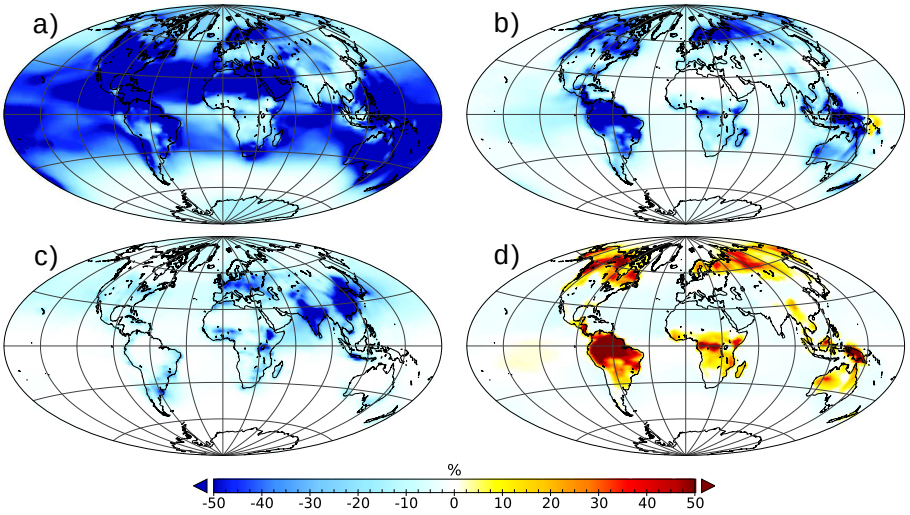

Fig. 2. Surface-level aerosol number concentration difference fields (%) from sensitivity simulations, due to **(a)** nucleation (NoNuc_BC12-ActNuc_BC12), **(b)** SOA formation (ActNuc_BC12_NoSOA-ActNuc_BC12), **(c)** black carbon emission size (ActNuc_BC24-ActNuc_BC12) and **(d)** nucleation parameterization (OrgNuc_BC12-ActNuc_BC12). Differences are calculated against ActNuc_BC12 simulation (Fig. 1).

ACPD
13, 26389–26450, 2013

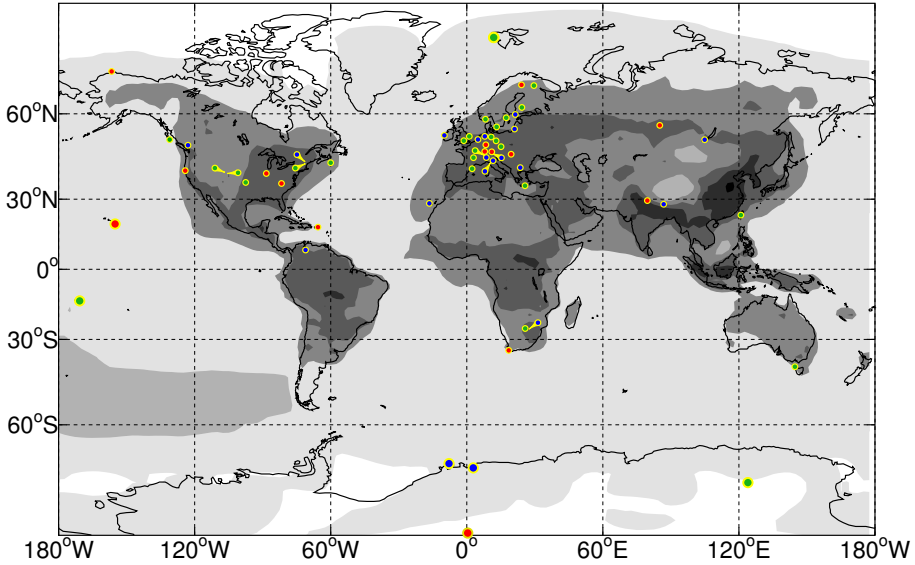

Fig. 3. Locations of the sites used in this study colored based on median number bias calculated from ActNuc_BC24. Red (blue) indicates a positive (negative) number bias higher than 20 %, while green shows stations with low bias (< 20 %). The background contour shows number concentrations from ActNuc_BC24 simulation.

ACPD
13, 26389–26450, 2013

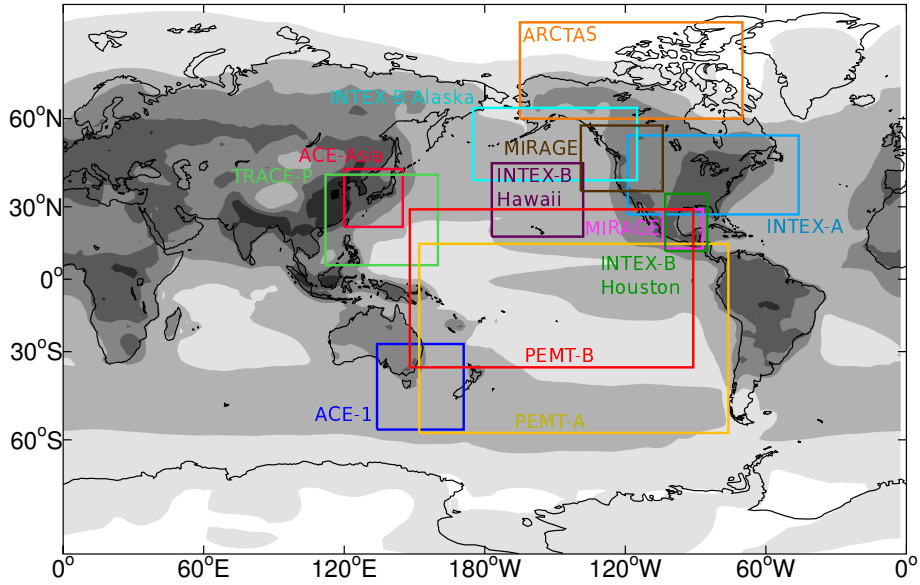

Fig. 4. Locations of flight observation campaigns used in this study. The regions and flight observation data is from Clarke and Kapustin (2010).

ACPD
13, 26389–26450, 2013

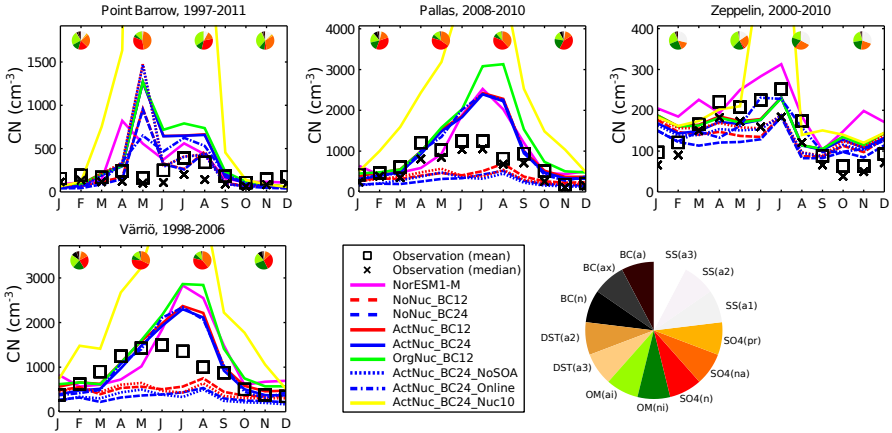

Fig. 5. Comparison against Arctic site observations. Line colouring is described in the legend. The pie charts indicate the relative contribution of components from NorESM simulations (ActNuc_BC24) in February, May, August and November. The years used for observation average is indicated on top of each panel.

ACPD
13, 26389–26450, 2013

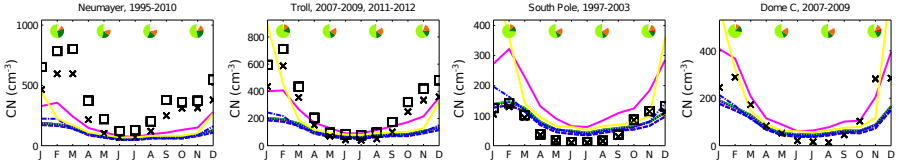

Fig. 6. As Fig. 5, but for Antarctic sites.

ACPD
13, 26389–26450, 2013

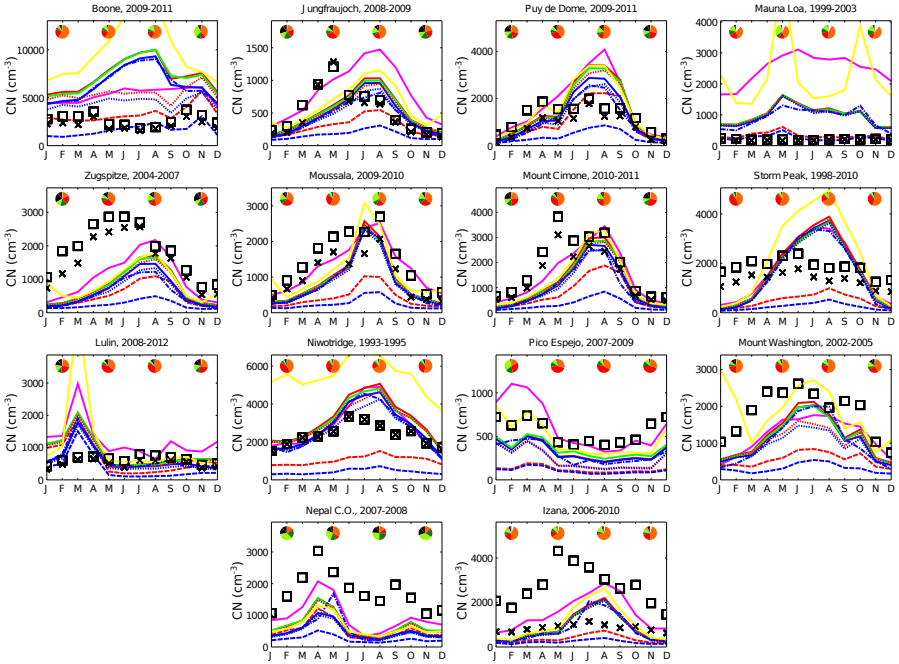

Fig. 7. As Fig. 5, but for high altitude sites (over 1000 m a.s.l.).

ACPD
13, 26389–26450, 2013

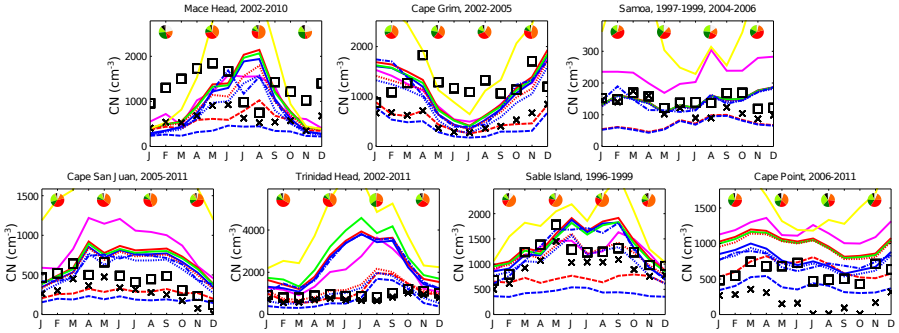

Fig. 8. As Fig. 5, but for marine sites.

.

ACPD
13, 26389–26450, 2013

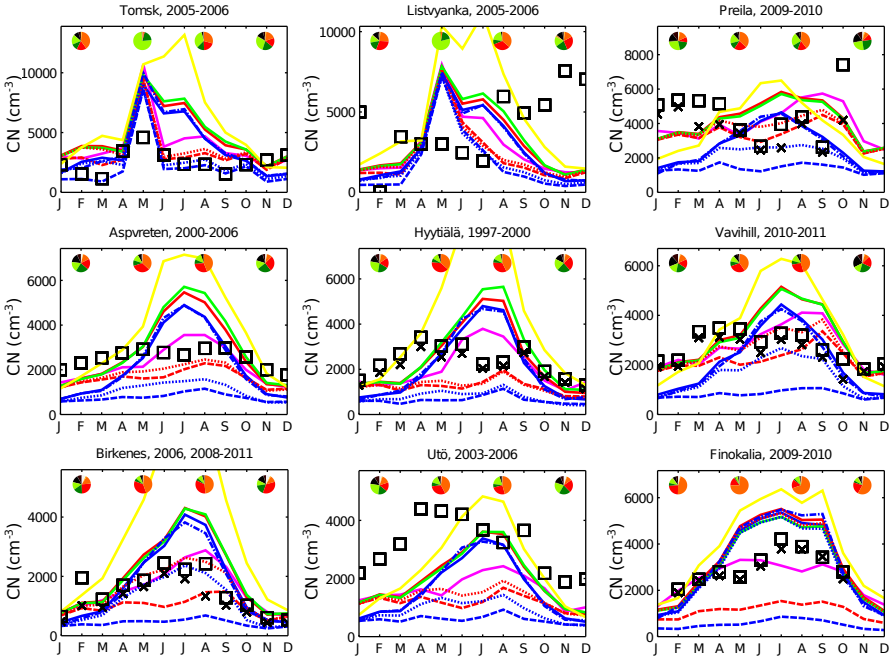

Fig. 9. As Fig. 5, but for remote sites.

ACPD
13, 26389–26450, 2013

NorESM aerosol number concentrations

R. Makkonen et al.

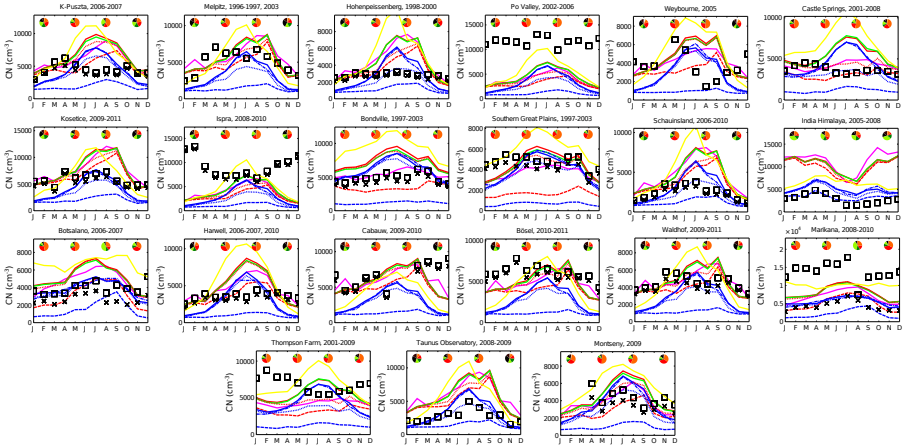

Fig. 10. As Fig. 5, but for rural sites.

ACPD
13, 26389–26450, 2013

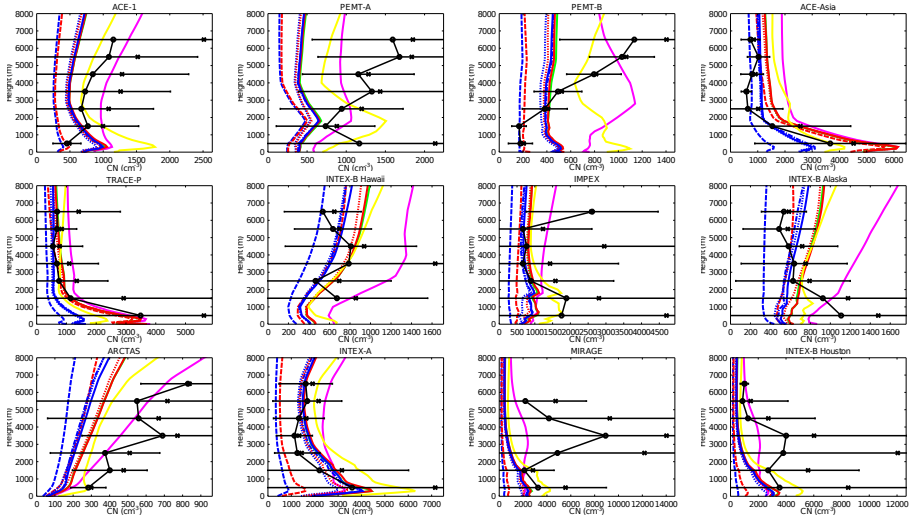

Fig. 11. Comparison of NorESM aerosol number concentrations against flight observations compiled by Clarke and Kapustin (2010). The observed median values (black circles) are surrounded by one standard deviation from observations. The observed mean value is denoted by black cross. The experiments are colored as in Fig. 5.

ACPD
13, 26389–26450, 2013

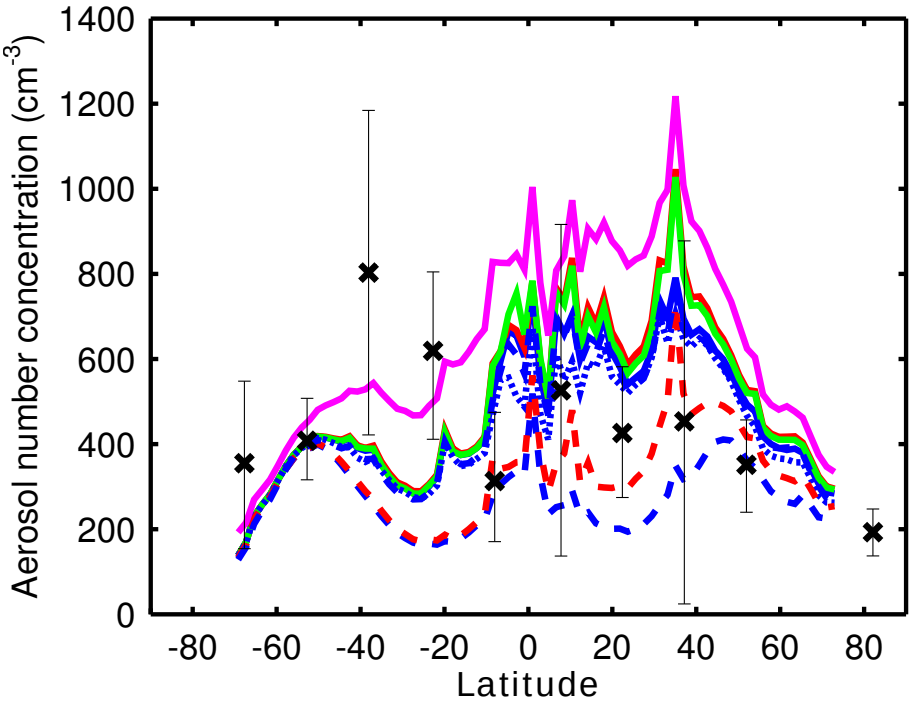

Fig. 12. Comparison of NorESM simulations against the dataset compiled by Heintzenberg et al. (2000). The model data is masked to include only remote oceans (see Suppelement Fig. S1). The experiments are colored as in Fig. 5.

.

ACPD
13, 26389–26450, 2013